Laser Remelting of Yttria Stabilized Zirconia Coatings Deposited by Suspension Plasma Spraying

Ashkan Baadi

A Thesis

In

The Department

Of

Mechanical, Industrial and Aerospace Engineering (MIAE)

Montréal, Québec, Canada

Presented in Partial Fulfilment of Requirements

For the Degree of Master of Applied Science (Mechanical Engineering)

Concordia University

Montreal, Quebec, Canada

December 2020

CONCORDIA UNIVERSITY

School of Graduate Studies

This is to certify that the thesis prepared

By: Ashkan Baadi

Entitled: Laser Remelting of Yttria Stabilized Zirconia Coatings Deposited by Suspension Plasma Spraying

And submitted in partial fulfilment of the requirements for the degree of

Master of Applied Science (Mechanical Engineering)

Complies with the regulations of the University and meets the accepted standards with respect to originality and quality.

Signed by the final Examining Committee:

_ Dr. Ali Dolatabadi_____ Chair

_Dr. Ali. Dolatabadi_____ Internal Examiner

_Dr. Pantcho Stoyanov_____ External Examiner

_Dr. Christian Moreau_____ Thesis Co-Supervisor

_Dr. Martin Pugh_____ Thesis Co-Supervisor

Approved by: _____

Dr. Mamoun Medraj, Chair of Department or Graduate Program Director

December 2020 Dr. Mourad Debbabi

Dean of Gina Cody School of Engineering & Computer Science

ABSTRACT

Laser Remelting of Yttria Stabilized Zirconia Coatings Deposited by Suspension Plasma Spraying

ASHKAN BAADI

CONCORDIA UNIVERSITY, 2020

Thermal barrier coatings (TBCs) are applied as a protective layer in a range of applications, mainly in the aero-engine and power generation industries to protect the metallic parts from high operating temperatures, especially in gas turbine-engines. One way to improve the efficiency of the engines is to increase the combustion temperature; in order to reduce potential damage to the metallic parts, TBCs are commonly applied to these components. The TBC comprises a bond coat and a top coat. Since Yttria Stabilize Zirconia (YSZ) has the best combination of properties among the various options, this material is most commonly used as the top coat on commercial TBCs.

The top coat in TBCs can be applied by different methods, including Electron Beam - Physical Vapour Deposition (EB-PVD), Atmospheric Plasma Spraying (APS) and the recently developed Suspension Plasma Spraying (SPS) which is one of the newest methods in applying top coat layers. SPS has the potential to generate columnar microstructures with a beneficial range of porosity: these columns reduce thermal stresses in the TBCs and at the same time provide an acceptable range of porosity which reduces the thermal conductivity of the coated layers. The columnar structure of this type of coating, despite having a potential to increase the life cycle of the top coat in terms of thermal stresses, can be a way of penetration for calcium–magnesium–aluminosilicates (CMAS) into the TBC structure, which will result in deterioration of the TBC.

In this thesis, the formation of a variety of top coats using Suspension Plasma Spraying SPS method is used in order to obtain the desired columnar microstructure. Subsequently, these layers are laser treated to study the possibility of creating a remelted layer across the TBC surface which should reduce the CMAS penetration. In this regard, advantages and disadvantages of the major laser parameters such as scanning speed, output power, power density and energy density were observed. Based on the experimental tests on columnar structures, it was found that increasing scanning speed and power does not have a linear relation and that increasing the laser travel speed above 2 m/min will cause nonuniform melting and create different phases on the surface of the substrate. At the same time, decreasing power below a certain amount will not cause significant changes to the substrate. A specific range of energy and power density need to be considered in order to obtain a uniform melted layer over the substrate.

ACKNOWLEDGMENT

First of all, I would like to thank god for the time given to me to spend in Concordia University, also I would like to express my sincere gratitude to Dr. Christian Moreau and Dr. Martin Pugh, for granting me an opportunity to be a part of this research, and who also guided me through the whole way. Not only their continuous support and encouragement during the research but also their compassion and leadership makes me so honored to be their student and taught me some lifetime lessons. It has been a great privilege to work with them and to learn from them.

I am so grateful to all Concordia Thermal Spray Research Center team members for their limitless support, especially Dr. Fadhel Ben Ettouil for his presence despite all the conditions he had and his availability to answer my most basic questions with patience. I would like to thank Dr. Navid Sharifi for his support during the research and wise solutions whenever it seems there will be no further steps and to all my great friends and group members for the great teamwork and their priceless friendship Saeed Grameh, Ali Nowzari, Hediyeh Khatibnezhad, Alexandre, Hafez, Elnaz, Behrad, Masiar, Morvarid, Farzam, Fariba and Omid for helping me throughout my master's program.

I extend my appreciation to Green Surface Engineering for Advanced Manufacturing (Green-SEAM) Network for the financial support and for providing a great platform to showcase our research work and to connect with many industries and universities from around the world.

Finally, I would like to thank my parents, for their unconditional love and brother and sisters through this way specially to my beloved brother Amir and my sister-in-law Laya supported me during the most complicated days of my life, since they have full faith on each single decision I made and in every single Step of my journey. I am also so grateful to receive full love and support from Dr. Dena Shamsollalhi who stood beside me through all the tough times and never let me

take a step alone and encourage me all over the way. This accomplishment would not have been possible without their everlasting support and invaluable love.

List of Contents

LIST OF FIGURES

LIST OF TABLES

LIST OF ABBREVIATIONS

APS	Atmospheric Plasma Spraying
BC	Bond Coat
CMAS	Calcium–magnesium aluminosilicate
CTE	Coefficient of Thermal Expansion
CVD	Chemical Vapor Deposition
DC	Direct Current
D-Gun	Detonation Gun
EB-PVD	Electron Beam-Physical Vapor Deposition
HVAF	High Velocity Air Fuel
HVOF	High Velocity Oxygen Fuel
PTA	Plasma Transferred Arc
PVD	Physical Vapor Deposition
SPS	Suspension Plasma Spray
TBC	Thermal Barrier Coating
TC	Top Coat
TGO	Thermally Grown Oxide

LIST OF SYMBOLS

S_t	Stokes Number
$V_\perp$	Normal velocity
$V_\parallel$	Lateral velocity
ρ_p	Particle Density
d_p	Particle diameter
v_p	Particle velocity
l_{bl}	Thickness of the flow boundary layer
μ_g	Plasma gas molecular viscosity
P_{out}	Output power
d	Spot size
P_d	Power Density
E_d	Energy Density
v	Scanning Speed

1. INTRODUCTION

1.1 THESIS OUTLINE

This study covers the effect of laser remelting on the structure and characterization of Yttria Stabilized Zirconia TBCs sprayed by the suspension plasma method, aiming to obtain a dense remelted layer with a network of perpendicular cracks on top of a columnar porous SPS structure.

The thesis will be presented in six main chapters, as follows:

Chapter 1 - Introduction: This chapter is dedicated to the background and motivation of the project. First, applications of TBCs and their structure are introduced; this will be followed by reviewing significant properties in selecting materials for TBCs and the techniques by which YSZ-TBC can be applied. Then, studies carried out regarding laser modification techniques and their related effects will be introduced. Additionally, the research objectives and concerns for this study are stated in this section. Finally, the scope of the work and limitations of this research are discussed in this chapter.

Chapter 2 - Literature Review: In this chapter, some significant research dedicated to suspension plasma spraying, laser treatment methods, conditions, and related influences are reviewed.

Chapter 3 - Experimental Methods: In this chapter, the experimental procedures, including substrate preparation, suspension preparation, axial suspension plasma spray conditions, and the laser treatment process used in this project will be presented in detail.

Chapter 4 - Results & Discussion: This chapter covers two significant sections. During the first section, observations and comparison of different SPS microstructures which are generated under a variety of conditions will be reviewed: in the following section, the effects of varying laser parameters on the SPS microstructures obtained from the first section, will be discussed.

Chapter 5 - Conclusion: In this section, a summary is made of all observations, comparisons, and tests from the previous chapter and conclusions are presented.

Chapter 6 - Future Work: In this chapter, future potential studies in this research will be discussed.

1.2 BACKGROUND AND MOTIVATION

1.2.1 Coating

Coatings are applied on the surface of industrial parts in various materials aiming to improve the performance and extend the component life against corrosive environments and thermal and mechanical shocks and stresses [1].

Coating differences and their performances depend on the environment in which they are going to be used. These processes are generally divided into two main categories: thick and thin-film coatings. In thin films, coatings have thicknesses less than one hundred microns, commonly obtained by chemical vapor deposition (CVD) or physical vapor deposition (PVD). On the other hand, thick film coatings have thicknesses from one hundred microns up to several millimeters. They can be applied by different coating methods such as chemical/electrochemical plating, brazing, weld overlays, or thermal spraying [2].

Coatings are used in many industries and for different applications such as aerospace, land-based turbines, automotive applications, marine, electronic materials and devices, medical and corrosion control, and metal processing [3].

1.2.2 Thermal Barrier Coatings

Thermal barrier coatings have been used as a protective layer in the gas turbine industry since the 1950s. This type of protection is applied in many sectors, mainly in the aero engine and

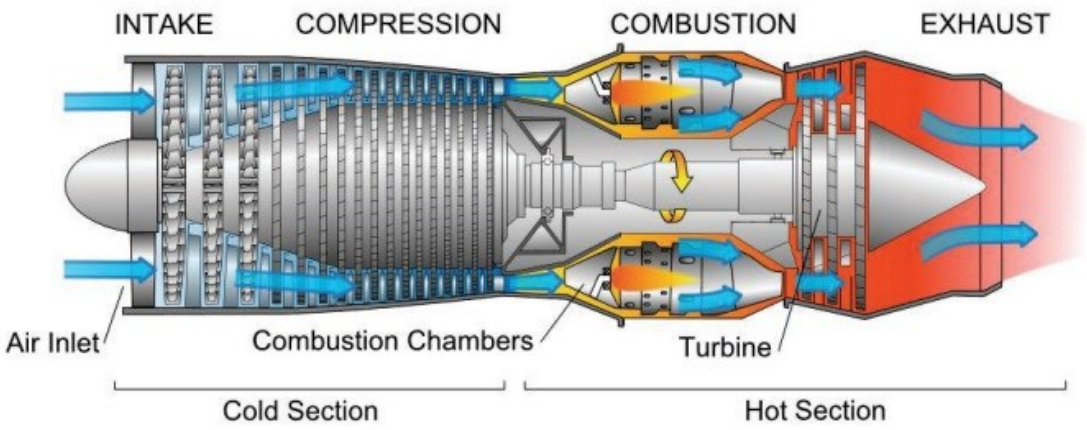

Figure 1-1 Example of gas turbine configuration [4]

power generation industry, to protect the metallic parts from high applied temperatures [4].

In aero engines, efficiency directly relates to combustion temperature. The maximum possible operating temperature is limited by the resistance of the Ni-based parts of the engine such as combustor, turbine blades, and vanes, and the afterburner (Figure 1-1) to these temperatures. Thermal Barrier Coatings overcame this problem and allowed higher operating temperatures and enabled the industry to reach a higher efficiency [5].

It is necessary to consider some fundamental properties to select a TBC material, such as a high melting point, no phase transformation (and associated volume change) between room temperature and operating temperature, low thermal conductivity, chemical inertness, thermal expansion match with the metallic substrate, appropriate adherence and low sintering rate of the porous microstructure. Yttria stabilized zirconia (YSZ) has a high coefficient of thermal expansion (CTE) for a ceramic and low thermal conductivity, and a relatively high melting point of 1200°C; these are the reasons why this material is the standard material of TBC topcoats [6].

A TBC is a multilayer coating system; a bond coat (BC) is a mid-layer between the substrate and the topcoat (TC). The bondcoat typically decreases the mismatch in thermal expansion

coefficients (CTE) between the substrate and the topcoat; overlay bond coats are usually MCrAlX-type in which M is Ni, Co, Fe, and X is an active medium with oxygen such as Y, Si, Ta, Hf. [4].

The second layer in a TBC system is the TGO (Thermally Grown Oxide) layer. During operation a TGO is formed due to oxidation of the bondcoat [7].

Lastly, the final layer of a TBC structure is the top coat (TC). This layer creates the primary insulation between the hot gas produced in the engine and the substrate. As was earlier highlighted,

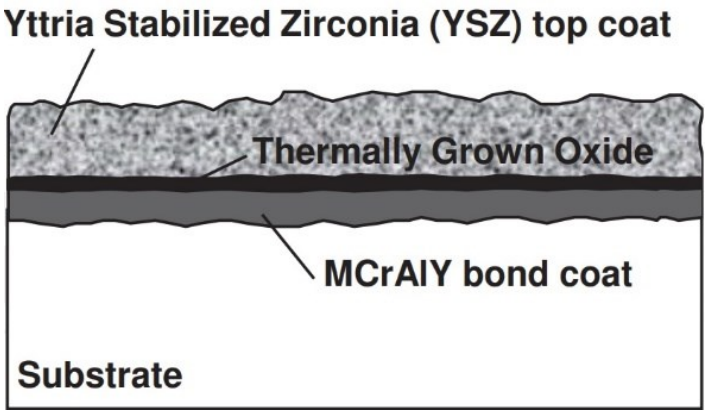

Figure 1-2. Schematic of Thermal Barrier Coating layers [38]

the selection of material for this part has some criteria, and yttria stabilized zirconia is selected due to its unique properties, such as low thermal conductivity(2.25 $W\ \mathrm{m}^{-1}\ \mathrm{K}^{-1}$) in bulk form, good mechanical properties, and good phase stability up to 1200 ^{o}C [8] [9]. The density of YSZ is about 6.0 g/cm^{-3} and it has a relatively high thermal expansion coefficient CTE is $11 \times 10^{-6}\ K^{-1}$, which is close to that of steel, for example ($14 \times 10^{-6}\ K^{-1}$) [10]. A close CTE decreases stresses from thermal expansion mismatch but still is a possible reason for thermal stress and crack propagation in the topcoat. The existence of porosity and cracks and/or a columnar structure reduces thermal stress levels and increases strain tolerance [11]. Robert Vaßen et al. have reviewed some potential materials to improve topcoat properties [8].

The two most widely used methods to apply TBCs are Electron Beam-Physical Vapor Deposition (EB-PVD) and Plasma Spraying.

1.2.2.1 Physical Vapor Deposition

A method of producing thin-film coatings is Physical Vapor Deposition (PVD). This process generally occurs in three steps:1) creation of vapor phase species, 2) transport from source to substrate, 3) film growth on the substrate [12]. This method includes many subcategories. One form of PVD that is utilized to coat the TBC layer on blades and vanes used in gas turbines is Electron Beam Physical Vapor Deposition or EB-PVD. In this process, a high-energy electron beam evaporates ingot materials in a vacuum chamber to subsequently condense them on the surface of substrate [13]. Using this method helps us to obtain different coating structures such as dense, columnar structures.

1.2.2.2 Thermal Spray

Thermal spraying was invented by a Swiss engineer, who used it to deposit lead and zinc as protective materials. In general, thermal spraying consists of different coating processes in which metallic or non-metallic material is transferred in the molten or semi-molten condition and deposited on a substrate to form a coating. [3]

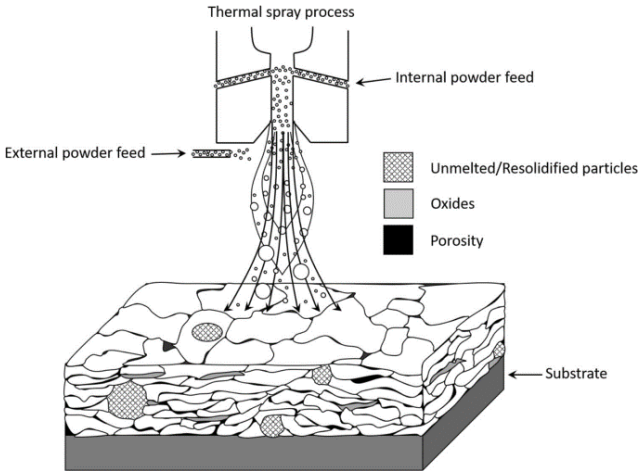

Figure 1-3 Thermal spraying schematic [3]

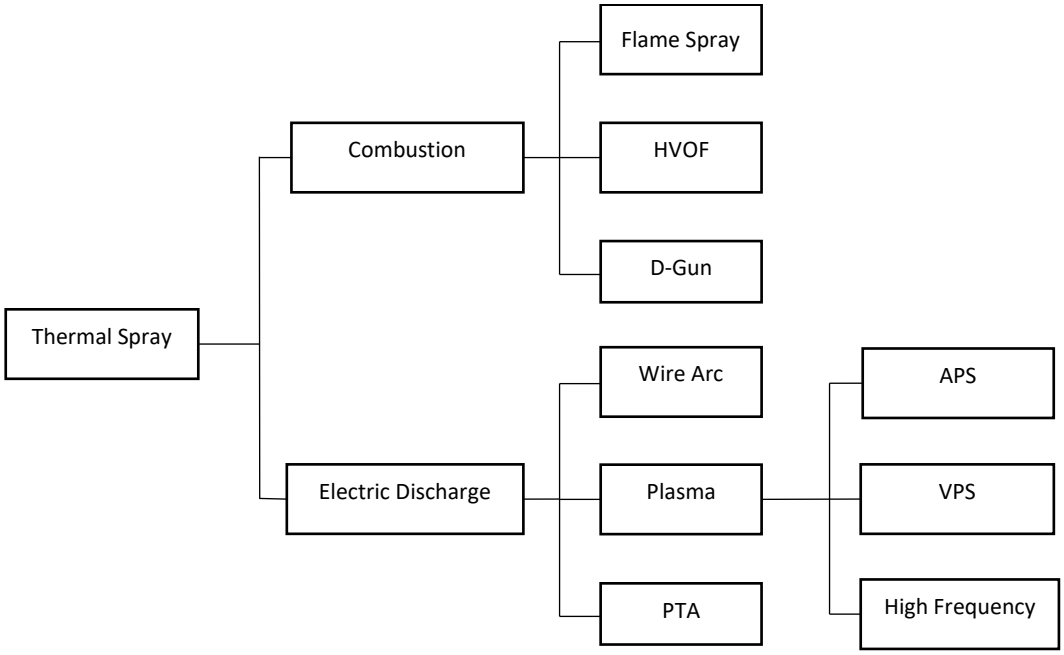

Figure 1-4. Classification of thermal spray technology [1]

In this process, the formation of a firm bond between the molten and/or semi-molten particles, which have high kinetic and thermal energy, with the substrate produces a cohesive coating [1] [2] [3].

Figure 1-4. illustrates the classifications of the various thermal spray methods. Particles are sprayed via thermal spray in different ways; flame spray, HVOF, D-Gun, wire Arc, PTA, and plasma spray. Among all these thermal spraying methods, "plasma spraying" is probably the most generally used coating process [1].

In plasma spraying, the coating material in particulate form is injected into the plasma flame to be heated to high temperature and accelerated towards the substrate. Plasma generation is an application of gas ionization [14]. A DC arc heats an inert gas. In this process, the heat source is an electric arc created by a cathode and anode [15]. High plasma temperatures heat and can melt the particles and then rapid solidification of molten and semi-molten material after impacting the substrate forms the material into splats. The deposition of these splats over each other creates the coating layer [3][16]. This process is known as APS (Atmospheric Plasma Spraying). Many factors affect the coating microstructure, which includes the spraying conditions and particle size used during the spraying. These parameters need to be controlled in order to tailor the coating microstructure. Spraying fine powder particles ranging from 1 nm to 100 nm results in a coating with a fine microstructure [15]. The main challenge in using fine particle size powders is to ensure the small, light particles penetrate into the plasma. The carrier gas has to have a high flow rate to impart a sufficiently high momentum to the particles. Therefore, the best way to inject small particles is to disperse the powder in a liquid carrier [14], known as the suspension plasma spray method (SPS). SPS is a relatively new coating method in plasma spraying, and has shown high potential to provide diverse microstructures with a broad porosity range.

One of the potential advantages of TBCs produced by SPS is the generation of a columnar coating structure. This columnar structure enhances the durability of the SPS coating by improving the stress relief mechanism in the coating. Additionally, due to its porous microstructure, it has a low thermal conductivity as well. These properties increase the lifetime of the coating. The performance of TBCs obtained by different methods such as APS, SPS, and EB-PVD techniques has been studied by Bernad et al. [17] and they concluded that SPS has potential to provide higher quality coatings.

1.2.3 Surface Treatment Methods

The structure of the TBC obtained by suspension plasma-spraying contains segmented cracks, high porosity with mostly interconnected pores, horizontal microcracks and pores open to the surface due to rapid cooling of molten droplets [18]. These defects are paths that can allow corrosive gases and molten salts to attack the lower layers, and this is magnified especially in the case where low purity fuels are used. The above-mentioned features affect the mechanical properties and the oxidation and corrosion resistance of these types of TBCs. To improve the service life of the coatings, different types of modification methods have been used, such as impregnation[19], sol-gel[20], hot isostatic press[21], chemical vapor deposition thin film[22][23], and laser treatment. However, selecting a specific technique depends on the required microstructure, composition, thickness, environmental impact, and economic viability[24].

The word 'LASER' stands for "Light Amplification by Stimulated Emission of Radiation,". It was first developed by Miaman [25] in the 1960s and was a breakthrough in science. This invention has been considered as the answer to many scientific problems and limitations in many fields. One of the areas which benefited from the innovation and development of lasers was

material processing starting in the 1970s when commercial lasers were starting to be utilized [26]. The laser has revealed a high potential for improving plasma-sprayed coatings by modifying some properties such as surface roughness, sealing open porosity, and generating a controlled segmented crack network. [27].

1.3 OBJECTIVE AND RESEARCH QUESTIONS

In considering the novelty of suspension plasma spray (SPS) technology in the production of ceramic coatings for enhanced thermal barrier coating properties compared with other methods, an improvement of the coated microstructure is a major benefit. Using this concept, it directed this study to consider a new approach to improve the SPS structure. This research aims to investigate the influence of laser parameters in formation of the remelted layer potentially to modify some properties such as those mentioned above, namely; reducing surface roughness, sealing open porosity, and generating a controlled segmented crack network following the microstructure of the columnar SPS coatings. Re-melting and fast solidification of a thin layer of YSZ on the top of the coating creates a dense, smooth re-solidified layer. This method can improve the protection of the bondcoat and substrate against CMAS (Calcium–Magnesium Alumino-Silicate) penetration; also, it will enhance the coated layer's life cycle and reduce the roughness of the coated surface, which has a direct effect on the flow turbulence over the topcoat.

1.4 THE SCOPE OF WORK

The first step of this work is obtaining a YSZ columnar microstructure with the SPS technique using different suspensions. These are applied to substrates with a range of surface roughness. During the second step, the effects of a 4 kW Continuous Wave fiber laser on the top layer of the coating's microstructure are studied in order to modify the top surface of the yttria partially stabilized zirconia TBC. This method may potentially improve the coating quality by protecting the bondcoat and substrate against CMAS penetration and potentially improve surface roughness (Figure 1-5).

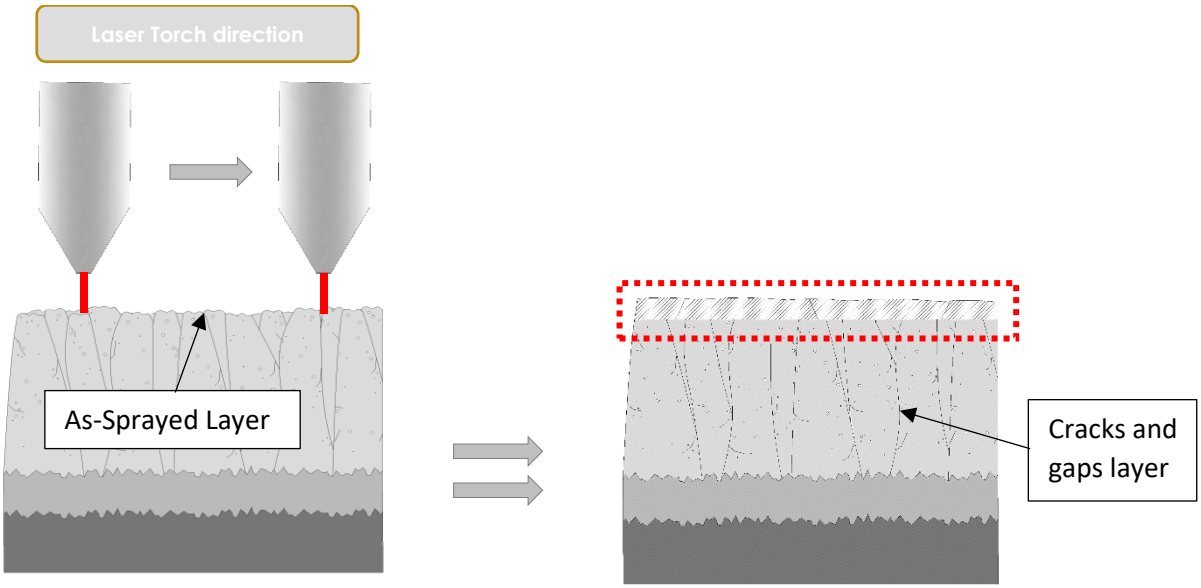

Figure 1-5 Schematic of laser treatment of columnar structure of SPS coatings

2 LITERATURE REVIEW

2.1.1 Suspension plasma spray

Suspension spraying is a relatively new technique in producing coatings with a variety of microstructures [16]. A liquid feedstock is injected directly into the plasma plume [28]. In this method, submicron or nano-sized powder particles are mixed at a specific ratio with a liquid medium to form a suspension. The dispersion of the submicron particles in the solution may be hindered by some agglomeration. This problem can be reduced by adding a small portion of a surfactant to reduce the agglomeration as much as possible. It should be noted that this amount should be calculated in a way not to affect the final result of the process [11].

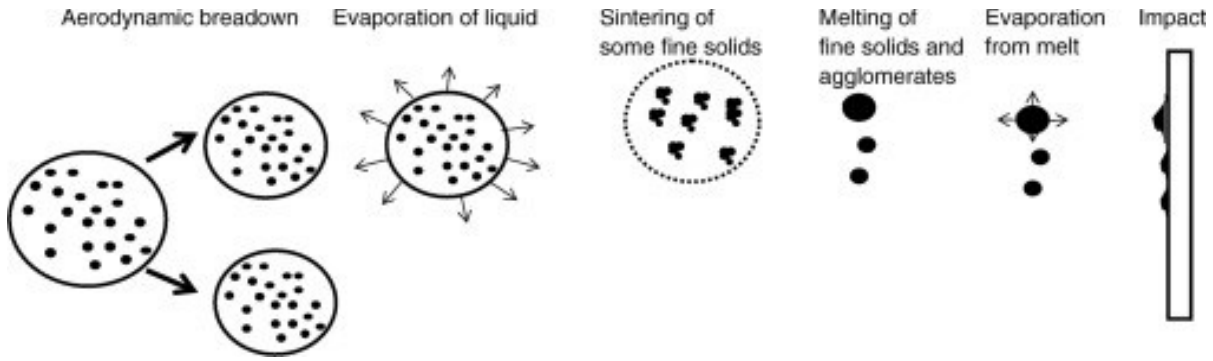

Figure 2-1 Transformation of suspension droplet in the plasma jet [15]

The prepared suspension is finally injected into the plasma to apply the coating layer [28], [29]. As a result of the plasma plume's temperature, the liquid carrier evaporates and fine particles are exposed directly to heat. This phenomenon will cause partial or full melting of these fine solid particles (Figure 2-1). These fine particles impact on the substrate to form a coating [15].

According to the operating parameters, such as plasma properties, suspension properties, substrate characteristics, plasma gas mixture, torch design, and stand-off distance, different structures may be formed in the coating [30]. SPS has a unique capability to produce a porous and columnar microstructure; this enables the coating to relieve thermal shock stresses and obtain a more extended lifetime; simultaneously, it has lower thermal conductivity. Therefore, numerous studies have been devoted to identifying the parameters responsible for the formation of the SPS columnar microstructure. VanEvery et al.[31] justified the columnar formation of SPS coating based on particle trajectories by a "shadow effect." Using different particle sizes, they showed that a lower weight percentage of nanopowder creates the random orientation of lamellae columns, separated by linear porosity bands. By increasing the amount of suspension, interconnected porosity bands were observed. This issue indicates that drag and inertial forces were different for different YSZ droplet size resulting in various types of spray deposition.

The smallest particles follow the plasma jet trajectory close to the substrate. They impinge on its surface with a strong parallel velocity component. Finally, the coating results in both lateral and normal growth around the asperities to generate columnar features.

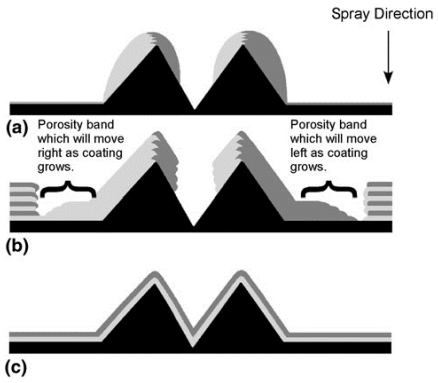

Figure 2-2 Deposition characteristics on asperities of the substrate [29]

B. Bernad et al.[70] utilized VanEvery's theory to formulate the evolution of column width in the columnar microstructure using normal velocity $(V_{\perp})$ and lateral velocity $(V_{\parallel})$ components: they reported that decreasing the normal component of velocity, $V_{\perp}$, has a direct effect on the creation of a more uniform and compact microstructure. By reducing the coating deposition rate on each pass without changing plasma conditions, nor suspension load, nor feed rate and only by increasing the linear velocity, $V_{\parallel}$, the $V_{\perp}$ normal velocity component will be reduced

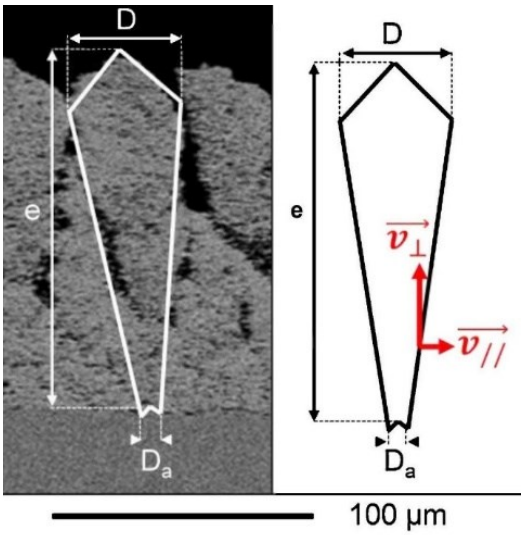

Figure 2-3.Columnar features and inter-columnar voids and cauliflowers formation [30]

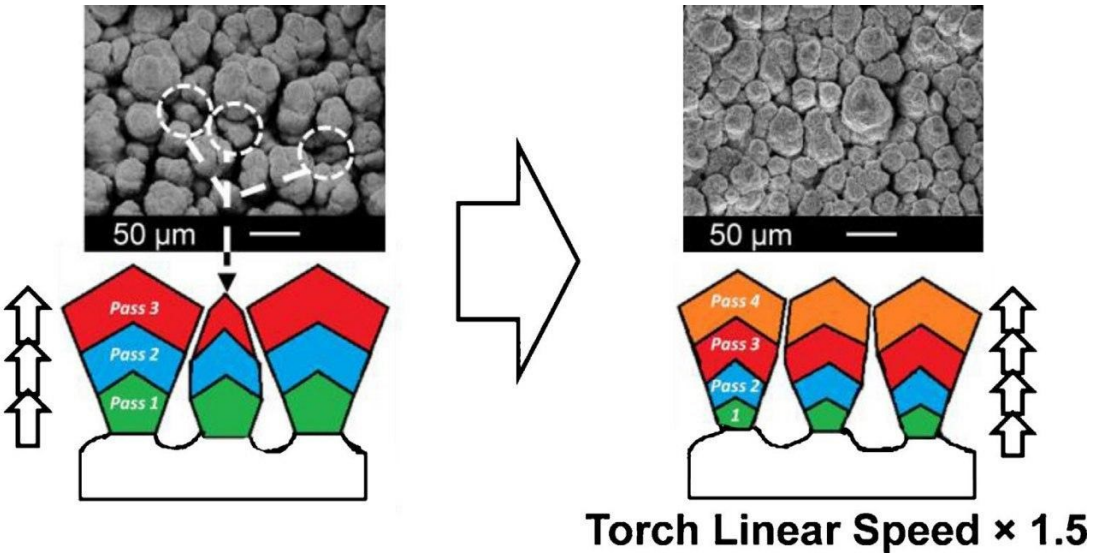

Figure 2-4. Linear torch speed effect on coating microstructure [30]

Substrate roughness is always considered as a critical parameter in the formation of the columnar structure. Fernanda Caio et al. [32] investigated the influence of substrate shape and roughness on SPS coating microstructure. They observed that an increase in the substrate's roughness on a flat sample resulted in increasing the formation of columns with wider thickness. This finding was a confirmation of the work of Bernard et al.[17] Different topographies were studied based on the roughness of the surface and this resulted in different column sizes. Several studies reviewed the effect of substrate roughness on the microstructure of the coating with various methods such as grit blasting and laser surface preparation [33], as well as variation in bondcoat roughness [35]. They generally confirmed that increasing the roughness of the substrate has a positive effect on the formation of columns.

Another significant parameter on the coating microstructure is the energy of the plasma and gas flow composition. In this regard, Ganvir et al. [18][34] used different plasma powers and total gas flows. They found out that a lower plasma power and total gas flow reduce the atomization effect. Consequently, large ceramic droplets are created after evaporation of the solvent by increasing the power and total gas flow, resulting in stronger atomization.

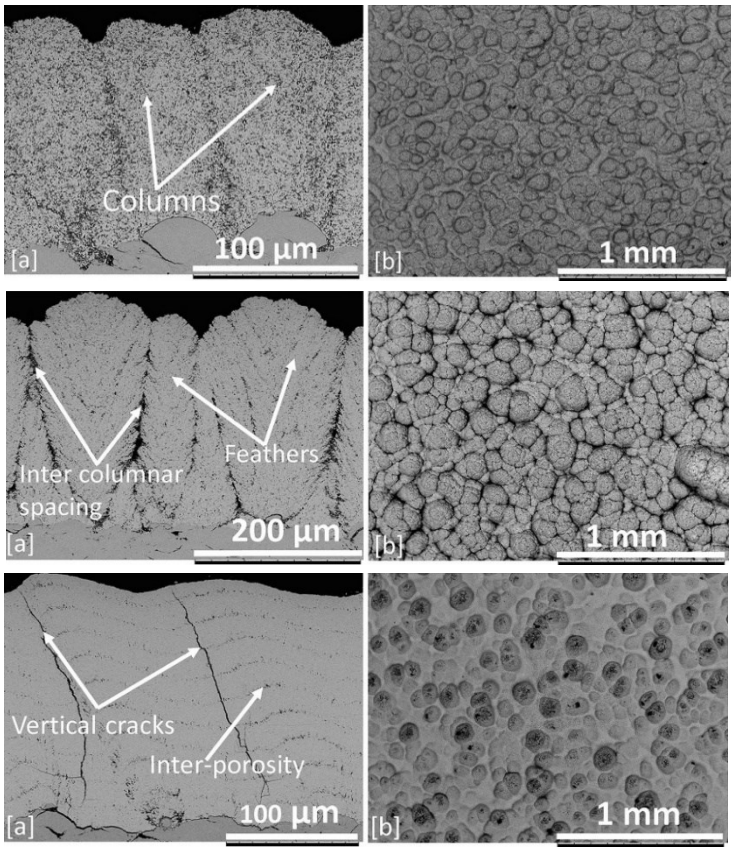

Figure 2-5. Cross section of different coating microstructure (a) Top view of the coating (b)

Another study considered the effect of torch power on the SPS coating microstructure of YSZ[35]. They found that increasing the torch power results in more thermal energy in the plasma plume. This has two significant effects: firstly, it increases the particle temperature which facilitates atomization and finer particles are introduced into the plasma, and the shadow effect is increased. The second effect is that higher torch power presents more energy to the atomized particles. More flying particles are melting thus a denser microstructure is generated at higher power.

Feed rate also has a role in the formation of the microstructure of the coatings. Increasing the suspension feed rate within the plasma results in the reduction of available energy for each particle [36]. The distance between the torch and substrate also has a critical role in forming the microstructures. A higher stand-off distance causes particle with lower velocity to interact with

the substrate surface. A reduction in the momentum of particles and the influence of the plasma flow results in an oblique deposition and formation of columnar structures [37][38].

D. Zhou et al. [40] reviewed the effect of spraying distance and solid suspension content on the coating microstructure. Based on their study, spraying distance influences the coating structure. By increasing the spraying distance to more than 100 mm a columnar structure could be obtained on all surfaces and roughness tested [38]. This phenomenon can be explained by considering the Stokes number, which was stated by K. Vanevery et al. [31].

$$S_t = \frac{\rho_p d_p^2 v_p}{\mu_g l_{bl}}$$

μ_g, ρ_p, d_p, v_p and l_{bl}, are plasma gas molecular viscosity, particle density, particle diameter, particle velocity, and the flow boundary layer thickness respectively. Spraying distance effects were also reviewed by Tang et al. [39] who observed that at 50 mm to 100 mm stand-off distance and with appropriate surface roughness, columnar structures with different densities could be obtained.

Zhou [38] also reviewed the effect of the solids content of the suspensions in terms of effects on columnar structure formation and found out that by reducing the solids content from 10% to 5%, the amount of porosity and the formation of columnar structures in the coating were increased.

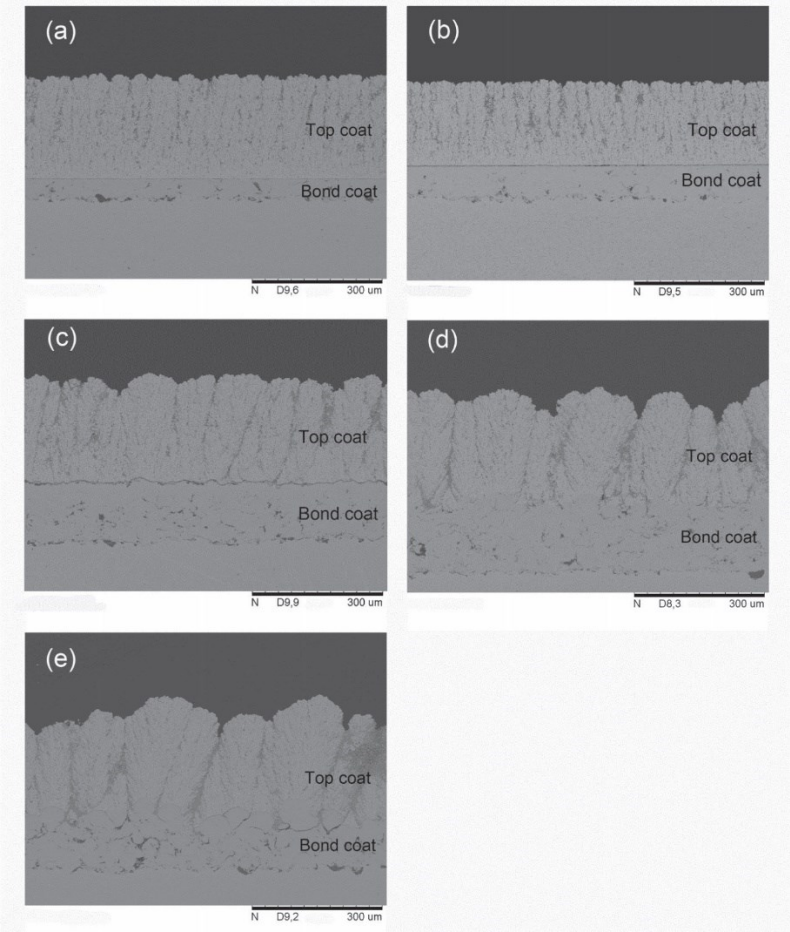

Figure 2-6. Effect of substrate roughness on the formation of columnar structure [38]

2.1.2 Laser Remelting Process

The columnar microstructure of the SPS coating is vulnerable in some aspects: for instance, the penetration of CMAS and oxygen into the cracks between the columns can cause severe damage in the subsurface layers. Also, increased surface roughness has a detrimental influence on the gas flow over the coated surface. TBC lifetime can be improved by various types of surface sealing. One of the most recognizable methods is laser remelting [40].

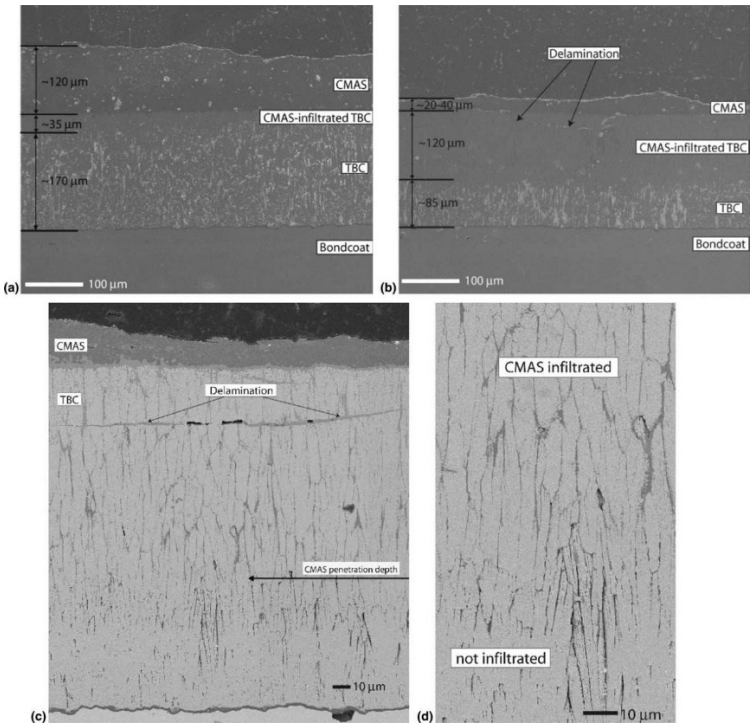

Figure 2-7. CMAS infiltration in TBC [40]

The standard process includes reheating, melting, and fast solidification of the melted zones resulting in increased TBC density at the surface, sealing of the surface holes and porosity, and a reduction specific surface area. Several studies have been carried out on the effect of laser remelting on plasma-sprayed TBC characterization and behavior.[41] Akdog˘an et al. [40] studied the impact of different laser power with a CO_2 continuous laser on the surface of plasma sprayed TBC, with the laser impinging for 10s on one spot. They increased laser power gradually to see the results in four different conditions. The results revealed that increasing power directly affects the thickness and width of the melted zone. Furthermore, based on the laser process parameters and the reduction in the surface roughness, a columnar structure with a controlled network of segmented cracks is formed, and this seals off sub-surface porosity.

Tsai et al. [42] used different settings for laser power, travel speed, and pulse frequency for both a continuous-wave laser and a pulsed laser to remelt a TBC sprayed by SPS. Batista et al. [43] treated the plasma sprayed YSZ thermal barrier coatings with a CO_2 continuous wave laser. Tests were carried out with a constant power of 500 W but at different scanning speeds as shown in Figure 2-8. The tests indicated that laser parameters such as scanning speed and track overlapping had a strong effect on the density of the segmented crack networks of YSZ, which are formed by the large and localized temperature gradients after the laser has passed. Additionally, using this method decreased the roughness of the as-sprayed layer and caused the creation of a fully dense columnar microstructure at the top of the layer. Another study by this group showed that the density of cracks oriented perpendicularly to the laser travel direction increases with increase in the laser scanning speed. [44]. Final surface examination suggests that coatings with a higher crack density, which are obtained due to increased scanning speed and overlap, have higher values of roughness [27].

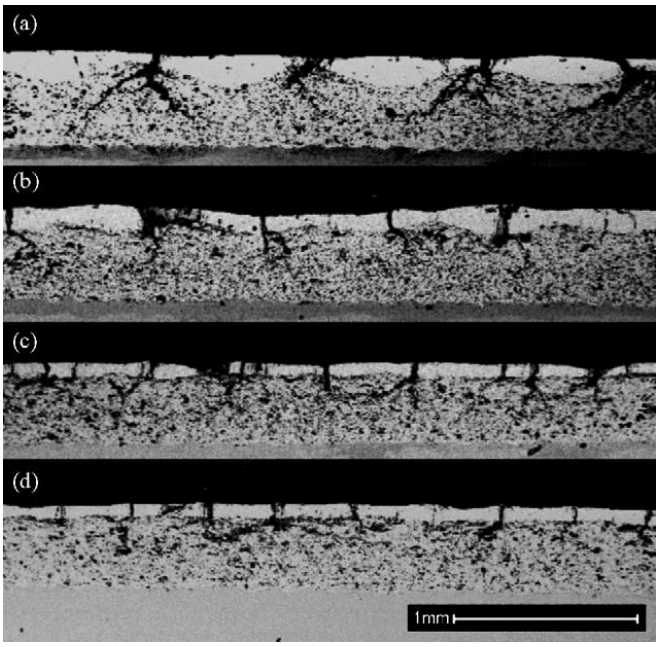

Figure 2-8. Cross section views of laser remelted layer, under a continous CO_2 laser with same power and different scanning speed [46]

These findings were confirmed by the study carried out by R. Ahmadi-Pidani et al.[45] which reported that laser parameters such as scanning speed, laser power, and frequency changed the segmented crack network of plasma-sprayed CYSZ.

Guven Gok et al.[46] used a 3 kW CO_2 continuous laser power to study the effect of different scanning speeds on the microstructure of a $Gd_2Zr_2O_2$ coating. Based on their research using the same power to melt the surface with different scanning speeds, they concluded that increasing the scanning speed reduced the remelted layer.

Morks et al. [47] used a continuous Nd: YAG 2 kW laser and they observed that after laser treatment, grains with different structures and sizes are generated. Mainly two-grain structures formed. The melting process occurred with the beam at a perpendicular angle to the asperities on

the sprayed coating surface. The diffuse reflection in the as-sprayed YSZ creates melted columns, solidifying with varying sizes of grain.

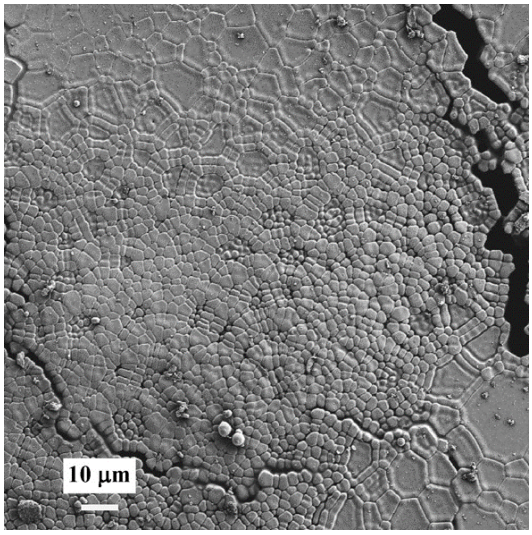

Figure 2-9. Surface deformation of re solidified layers [49]

Another aspect of laser re-melting process is the thermal shock resistance behavior of the TC microstructure. In a study carried out by Zhengjie Fan et al. [48], YSZ coatings formed by the APS method, were remelted with a Nd:YAG pulsed laser with different scanning speeds after which thermal shock tests were performed. They found out that thermal fatigue resistance is affected positively by having a small grain size in the structure: moreover, better compliance of stress during the movement of columnar grains is allowed in the separate columns. Yang Feng et al. [49] studied the thermal shock failure of TBCs by performing thermal cycling tests for both as-sprayed and remelted samples from the stress perspective such as phase transformation stress, growth stress, and thermal mismatch stress.

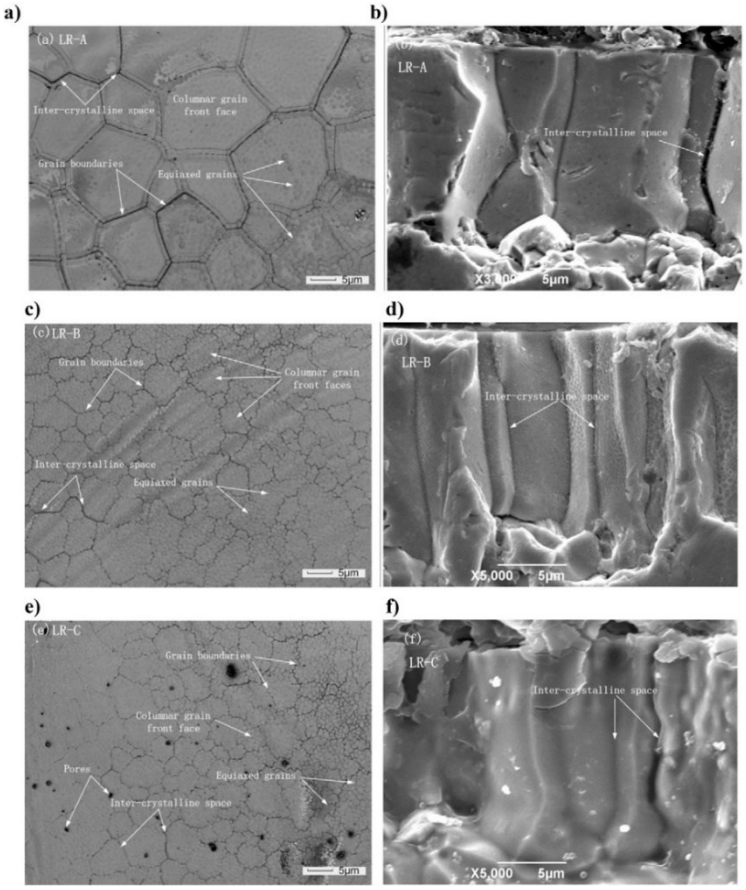

Figure 2-10. Surface and cross-section of columnar grain formation of remelted layer [51]

They concluded that the residual compressive stress in the as-sprayed YSZ TBCs was significantly higher than that in the remelted YSZ TBCs, which meant the failure mode in the as-sprayed conditions was delamination, whilst in the laser remelted samples, failure started from the edge. A lower thermal mismatch stress in the remelted YSZ TBCs, led to a lower spallation tendency of the TBCs.

Chen et al. [50] reviewed microstructural thermal shock behavior using a continuous laser on a newly formed structure. It revealed that changing the laser energy density altered the structure from a single columnar grain to a combination of columnar grains. This resulted in improved thermal shock resistance by improving the thermal expansion coefficient mismatch between the ceramic coat and metallic substrate.

Pi-Chuen Tsai et al. [53] reviewed the erosion resistance features using laser remelting of YSZ coatings. They used the APS technique to obtain the YSZ coating and a pulsed CO_2 laser for remelting. This laser-glazing process improved the microhardness compared to the as-sprayed layer and these results were confirmed by other studies [47]. Meanwhile, laser glazing improved the erosion resistance up to 3 times in comparison with the as-sprayed condition.

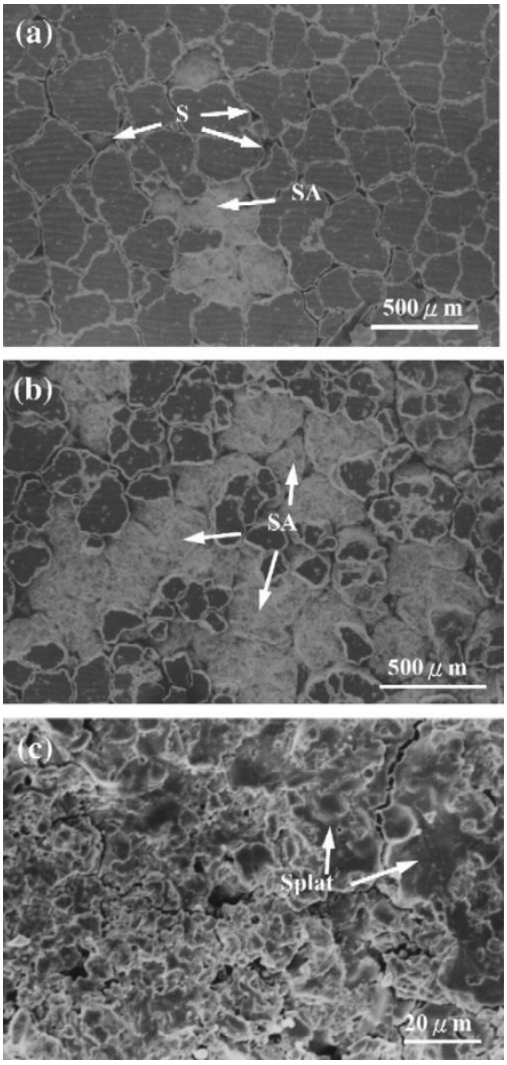

Figure 2-11 The eroded surface laser glazed TBC [53]

Another major aspect of laser remelting is the resistance of YSZ coatings against molten salt and CMAS penetration. Peng Yi et al. [51] remelted APS-YSZ top coats using a continuous-wave diode laser. Different laser parameters including the scanning rate, were applied to obtain the optimal TC remelted condition. The remelted surface was then covered with a salt mixture and subjected to a hot corrosion test. It was concluded that after creating a dense and smooth remelted layer, the hot corrosion resistance of the TC improved. Also, the infiltrability of the surface by the salt mixture was reduced. These results confirmed the study carried out by Ghasemei et al.[52].

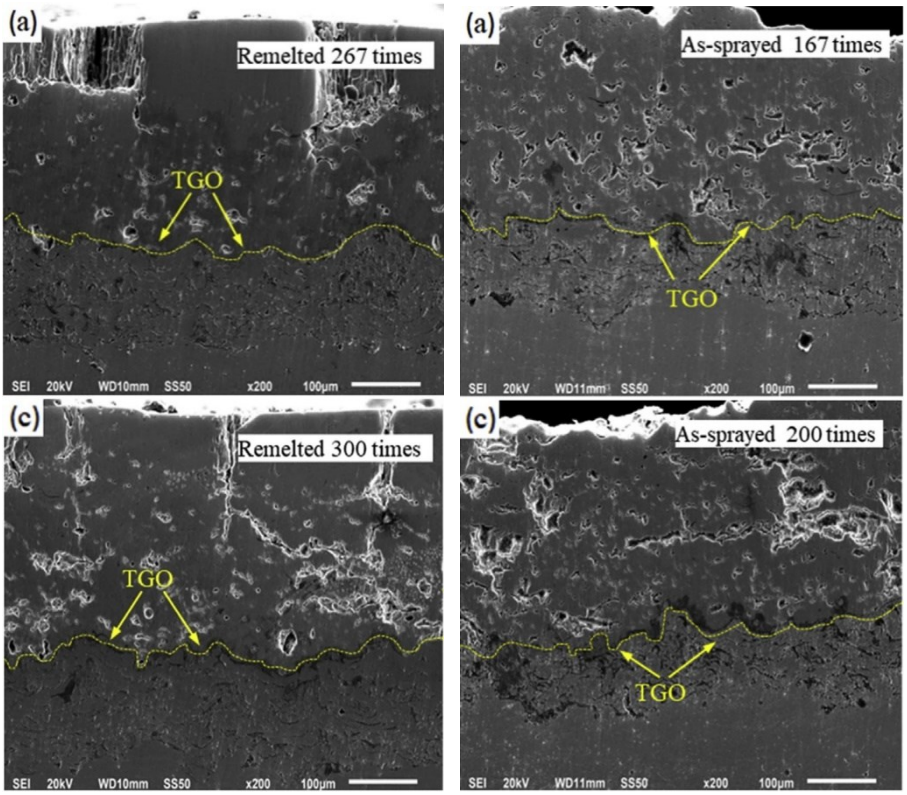

Figure 2-12 Cross section morphologies after thermal cycling [52]

Damage mechanisms of corrosion of remelted TBCs were studied by Zhengjie and categorized as the primary damage in their study. Also, they found out stresses stemming from YVO_4 growth in YSZ cause the spallation of the TBC. Also, excessive oxidation of the bond coating leads to degradation near the topcoat/bondcoat interface. In addition, molten salts would attack the columnar grain boundary exposed to the acidic environment, causing damage at these grain boundaries.

Zheng Yan et al. [53] studied the effects of laser remelted TBCs exposed to CMAS corrosion by optimizing laser parameters using a pulsed laser machine. Laser glazing changes the coating

microstructure, creating a dense columnar structure with a smooth surface and open channels consisting of vertical cracks and inter-columnar gaps. The laser-glazed part reveals improved CMAS resistance compared to as-sprayed coatings. The columnar structure remains the same, and desirable metastable tetragonal (t') phase after the CMAS attack stays stable. In contrast, both the as-sprayed coating and the coating beneath the glazed layer are seriously damaged.

3 EXPERIMENTAL PROCEDURE

3.1 SUBSTRATE PREPARATION

In this work, squared shaped coupons ($25.4 \times 25.4\ mm$) with a thickness of 3.5 mm were used as the substrate: these coupons were made of stainless steel 304.

As the first step, to remove any potential contamination such as dust and oil and produce a uniform surface of a specific roughness, the substrates were grit blasted in a blasting cabinet. The grit blasting pressure used was 100 psi unless otherwise stated.

To obtain different roughnesses, a variety of sizes of aluminum oxide (Al_2O_3) abrasives were used (International Surface Technologies, Montreal, QC, Canada), which are cited in Table-3-1 [54]. The presence of asperities on the substrate surface improves adhesion between the coating and substrate; additionally, it increases the shadow effect, which results in improvement of the creation of the columnar structures [1][8].

Due to the different alumina sizes used (Table 3-1), substrates with two different roughnesses were obtained. The substrate surface roughness (R_a) was computed with a Mitutoyo SJ-210 Series device.

Grit Blast	*Grade*	*Pressure (PSI)*	*Ra (μm)*
Aluminum oxide (Al_2O_3)	20	90	4.51
Aluminum oxide (Al_2O_3)	80	100	1.63

Table 3-1. Grit blasting parameters

Finally, the substrates were exposed to compressed air jets to remove embedded grit residue on the surface as much as possible. Once again, the substrate is put into an acetone solution to remove any impurities from the substrate's surface.

3.2 SUSPENSION

3.2.1 Components

The solid ceramic material used in this project is zirconium oxide (ZrO_2) powder (Changsha Huazun Ceramic Material Co, China) stabilized with 5 mol% (8 wt. %) yttrium oxide (Y_2O_3) for the in-house solution and Treibacher, Althofen, Austria 5 mol% (8 wt. %) yttrium oxide - zirconia for the commercial suspension.

From the literature, it is known that the carrier liquid has a direct effect on atomization [55]. Curry et al. [56] used water instead of ethanol and found out this increased the tendency to create vertical cracks in conditions similar to ethanol solvent. However, ethanol requires less enthalpy to vaporize in comparison with water [57]. As a result, ethanol was selected as the liquid carrier in this project.

To reduce any agglomeration in the in-house suspension, polyvinylpyrrolidone (PVP) was added as a dispersant to the suspension. The amount of PVP in the in-house suspension is 5% of YSZ weight in the total suspension. PVP is added, otherwise, due to electrostatic attraction the sedimentation rate increases, and also the PVP resists the temptation of YSZ submicron particles and oxides to create agglomerates [55]. To further avoid any agglomeration during the preparation, a Sonicator Q700 (Qsonica, Newtown, USA) is used at different stages, as noted in the following sections.

3.2.2 Suspension Preparation

In this project, two types of suspension were used: an in-house suspension and a commercial suspension. In preparing the in-house suspension, PVP was added to ethanol whilst being stirred by a magnetic agitator. To produce, a homogeneous and stable suspension, after adding 1-2 grams of PVP into the ethanol, the solution was stirred and sonicated with 70 W power for 3-4 minutes. This process was continued until all the PVP had been added to the ethanol. After adding the full amount of PVP to the suspension, the YSZ powder was added. For each 55-60 grams of YSZ added, 3-4 minutes of sonication were applied while the suspension was being continuously stirred. After preparation, the suspension mix was sonicated for an extra 25 to 30 minutes.

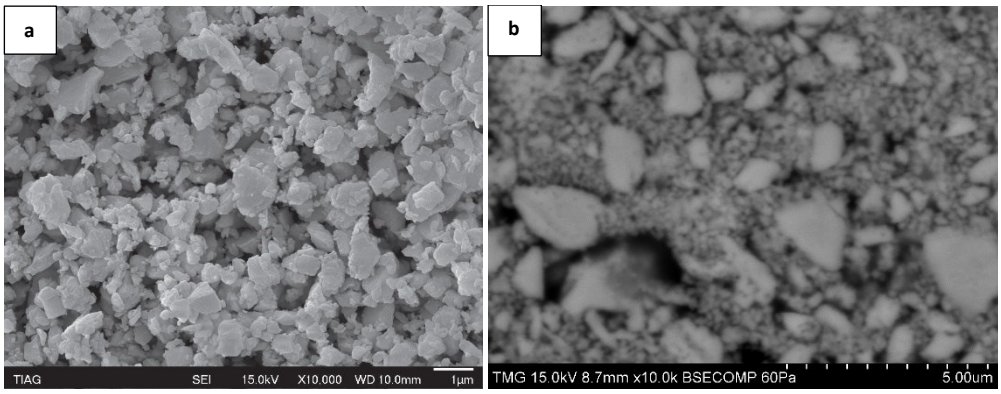

Figure 3-1. (a) YSZ primary particles in commercial suspension [58] (b). YSZ primary particles in in-house suspension

The commercial suspension is a pre-prepared mixture. Therefore, prior to spraying, the suspension bottle is continuously shaken for 5 to 10 minutes; afterwards, it will be ready to add to the feeder reservoir and proceed with the spraying.

The particle size distribution in the suspension is measured after preparation with a laser light scattering technique (Spraytec, Malvern, UK). The average particle size information is indicated in Table 3-2.

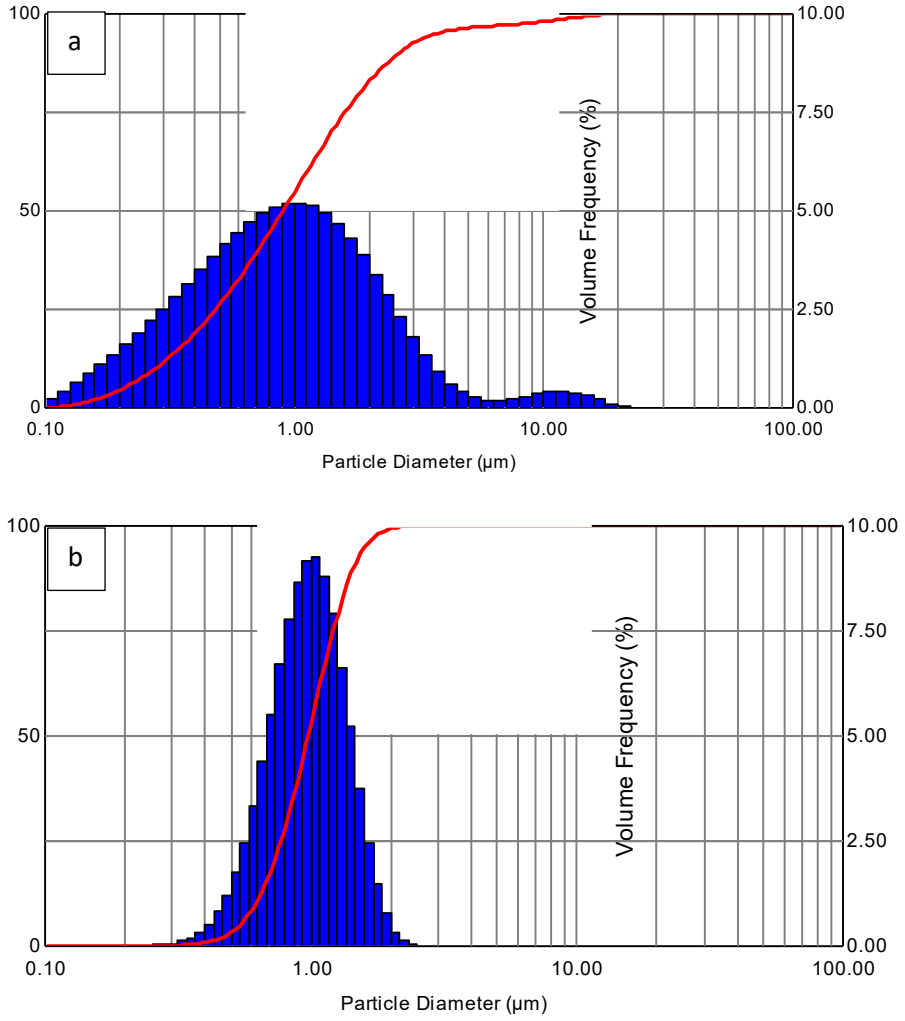

Figure 3-2. Partcle size distribution (a) in-house (b) commercial suspensions

SUSPENSION	SOLID CONTENT	PARTICLE DISTRIBUTION SIZE (µM)		
		$D_{v(10)}$	$D_{v(50)}$	$\mathbf{D_{v(90)}}$
IN-HOUSE (I-H)	25%	0.2769	0.9003	2.6120
TREIBACHER (T-B)	25%	0.6189	0.9725	1.4460

Table 3-2. Particle size distribution

3.3 SPRAYING AND REMELTING PROCEDURES

Due to the nature of this project, there are two stages of experiments:

1) Spraying process using the Mettech Axial III torch.

2) Laser treatment using the IPG laser.

3.3.1 Spraying Process using Mettech Axial III torch

3.3.1.1 Plasma Torch

In the spraying process, injection of the different droplet sizes results in different momentums as they enter the plasma stream; for instance, tiny droplets may not penetrate into the plasma. Optimum sized droplets may enter the core of the plasma. Finally, larger droplets may completely pass through. An axial injection is a solution to this problem. In this research, a commercial Axial III torch (Northwest Mettech Corporation, Vancouver, Canada) is used. This torch has three cathodes and anodes. Therefore, by a direct current arc, one unified plasma plume is generated inside the torch. In this torch, feedstock is injected into the center of the plasma and the flow axis. This mechanism keeps all the feedstock in the plasma plume and keeps them exposed to plasma heat before impacting the coating surface. As a result, this increases spraying efficiency [59][4].

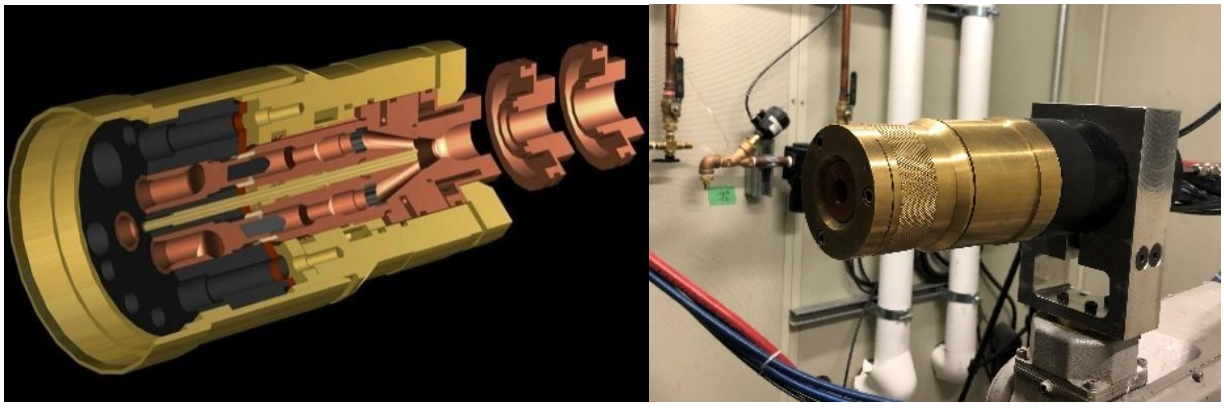

Figure 3-2. (a) Schematic of Northwest Mettech Axial III central injection torch [62] (b) Installed Axial III Mettech torch

3.3.1.2 Feeding System

A significant parameter in the SPS process is the "Suspension Injection", this parameter should be set to produce a homogeneous spray of solid particles in the plasma plume. The research suspension was injected from inside the nozzle by a Mettech Nano-feeder 350 (Northwest Mettech Corporation, Vancouver, Canada), which delivers the micron-scale particles into the thermal spray coating equipment [60].The suspension-feeding mechanism has a sealed tank in which the suspension is stored. The suspension is pumped into a tube connected to the center of the Mettech torch axis and is positioned so that the flow of the suspension jet is in line with the plasma jet. A mechanical stirrer can rotate in the suspension tank to avoid sedimentation of the solid content in the suspension during deposition.

Primary gas, which is argon, initiates the plasma, and the suspension will be injected into the system by the controller and with the introduction of the secondary gases ($H_2 + N_2$) the suspension atomization will be completed. It should be mentioned that the controller will adjust the feed rate. The continuous liquid jet penetrates the plasma plume. After fragmentation/vaporization, the YSZ particles are heated in the plasma plume, propelled toward the substrate, and form the coating.

3.3.1.3 Axial Suspension Plasma Spray Method

Two final deposition conditions were chosen for thermal spraying on the stainless-steel substrates. For each situation, both in-house and commercial suspensions were used for spraying on substrates prepared with the two roughnesses. The detailed information of spray conditions is stated in Table 3-3. Samples are categorized based on the suspension used during the tests:

commercial samples denoted by “T”, while samples sprayed using the in-house suspension denoted with an “M”. During spraying, two different feed rates were used: a high feed rate of 45 ml/min and a lower feed rate of 30 ml/min. In this research the samples produced with high feed rate are distinguished by “H” in the sample designation and low feed rate samples with an “L”. In addition, the substrate roughness varied from 1.6 µm to 4.5 µm in our samples and these roughness values will be named as “Smooth roughness” for 1.6 µm (labeled as “S”) and “Rough substrate” (labeled as “R”). To better understand the naming procedure please refer to Table 3.2. A sample made from commercial suspension at high feed rate on a rough substrate is thus named T-H-R.

T	Commercial suspension
M	In-house suspension
H	High feed rate
L	Low feed rate
S	Smooth substrate
R	Rough substrate

Table 3-3. Sample naming based on suspension, feed rate and surface conditions of different samples

On each round of spraying, six samples are attached to the sample holder as shown in Figure 3-5. The Axial III torch was mounted on a programmable robot (HP-20, Motoman, Yaskawa Electric Corp., Waukegan, IL, USA) to ensure the proper spraying process. The spray conditions that are controlled include: gas composition, viscosity, feed rate, and current. A separate Mettech controller controls the voltage.

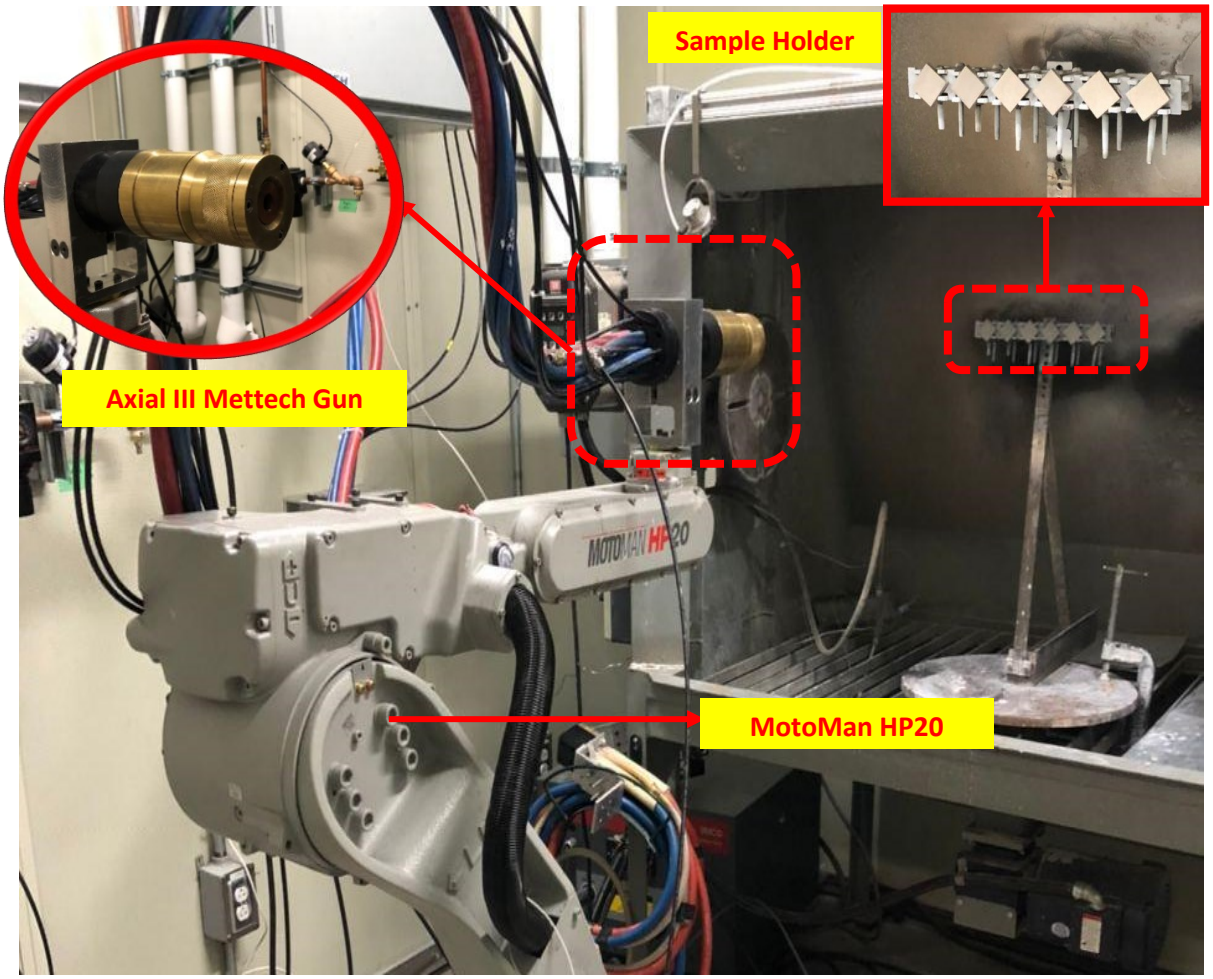

Figure 3-3. Suspension plasma spray process

Sample	*Grit Size*	*Substrate Roughness Ra (µm)*	*Power (kW)*	*Plasma Gas (L/min)*			*Total Gas (l/min)*	*Atomizing Gas (l/min)*	*Current (A)*	*Feed Rate (mL/min)*	*Robot Speed (mm/s)*	*Spray Distance (mm)*	*Number of Passes*
				Ar	**N2**	**H2**							
T-H-S	#80	1.63	101	50	30	20	260	15	180	45	1	100	20
T-H-R	#20	4.52	101	50	30	20	260	15	180	45	1	100	20
T-L-S	#80	1.63	101	50	30	20	260	15	180	30	1.5	100	40
T-L-R	#20	4.52	101	50	30	20	260	15	180	30	1.5	100	40
M-H-S	#80	1.63	101	50	30	20	260	15	180	45	1	100	20
M-H-R	#20	4.52	101	50	30	20	260	15	180	45	1	100	20
M-L-S	#80	1.63	101	50	30	20	260	15	180	30	1.5	100	45
M-L-R	#20	4.52	101	50	30	20	260	15	180	30	1.5	100	45

Table 3-4. Suspension plasma spray conditions. All solutions contained 25 wt% YSZ .

3.3.2 Laser

The TBC post-treatment was carried out with an YLS-4000-CT fiber laser (IPG Photonics Corporation, Oxford, Massachusetts, USA). The YLS is a single-mode ytterbium fiber laser, operating in continuous mode [61]. The laser has an emission wavelength of 1071 nm, with a 5.12 mm raw beam diameter, and a measured spot size of 3.2 mm [62]. To ensure security, an interlock system was installed so that the laser deactivates if the spray booth door opens. All the exit holes from the booth were sealed by custom-made plates, and the windows screened by laser curtains.

3.3.2.1 Laser Treatment Method

More than a hundred conditions were tested, and the optimized conditions were used for the final runs. Each sample was melted in four different conditions, noted as C1, C2, C3, and C4.

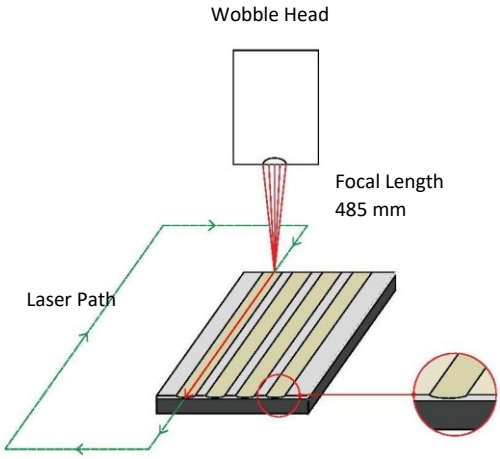

Figure 3-4. Laser remelting process schematic

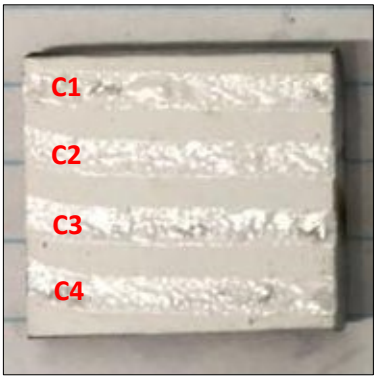

Figure 3-5. Remlted samples after four completed passes

The laser passed only once over the surface of our substrate under each condition. The main tests were carried out on six major sample sets with a total of twenty-four conditions. These samples are labeled as Test-19, 21, 22, 23, 24 and 25. The detailed information about the laser parameters and conditions applied for each sample are stated in Table 3-4. To perform this test, the Laser Wobble Welding head (IPG Photonics Corporation, Oxford, Massachusetts, USA) was installed on the programmable robot (HP-20, Motoman, Yaskawa Electric Corp., Waukegan, IL, USA). During the laser scanning, only one sample was placed on the sample holder for each test and to avoid any possible damage the robot was programmed in a way so that the laser head moves in a rectangular path (Figure 3-6), and activation time was set in

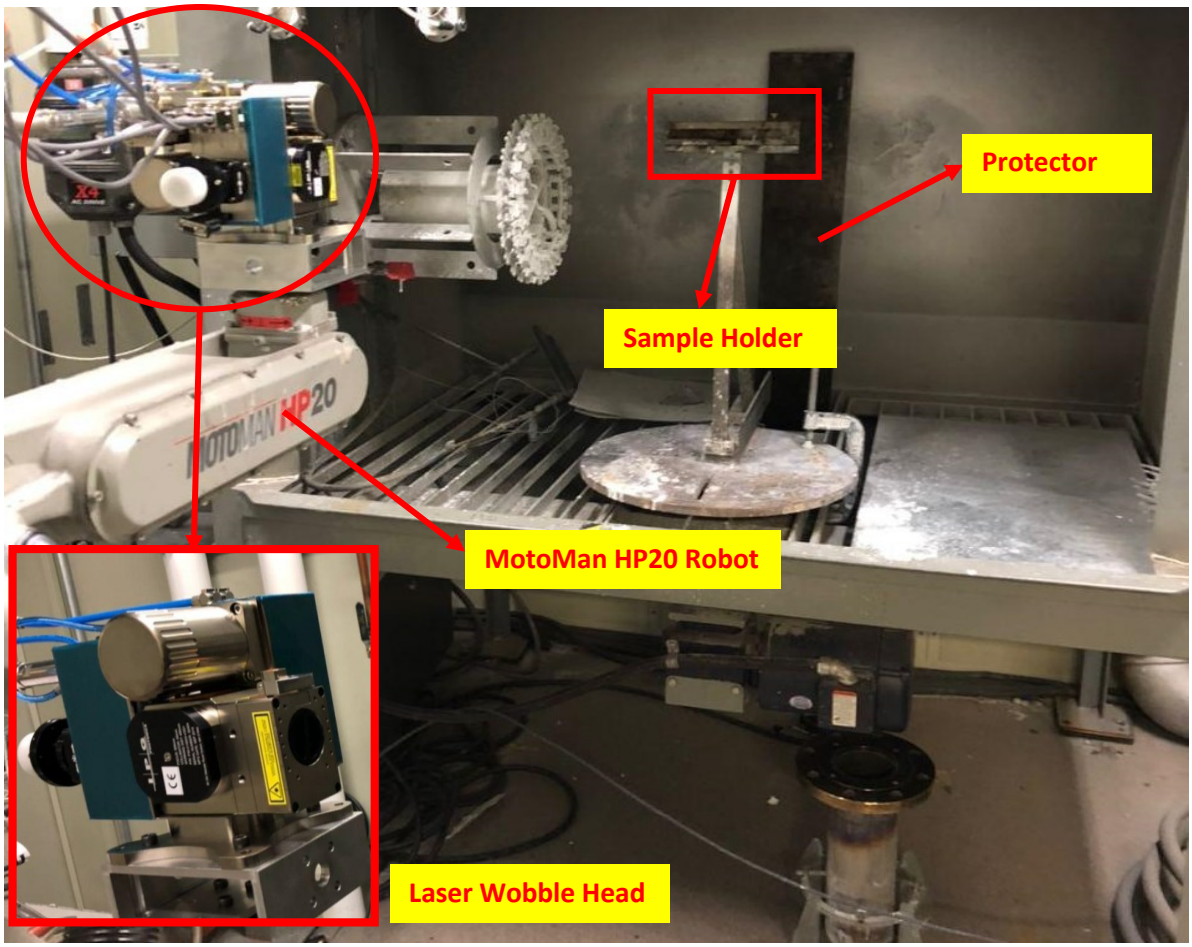

Figure 3-6. Laser remelting process and components

a way such that the laser was activated only during the period in which laser passes over the surface of the coated layer. Laser parameters and conditions are controlled by a local computer using IPG licensed software.

Test Number	Sample Label	Laser trace	Power (W)	Robot Speed (m/min)	Spot Size (mm)	Power Density (MW/m2)	Energy Density (J/mm2)	Melting Depth (μm)	Coating Thickness (μm)	Melting Percentage
Test 19	T-H-S	C1	1000	2	3.2	124.34	9.38	104.5	153	68%
Test 19	T-H-S	C2	800	2	3.2	99.47	7.50	32.9	153	22%
Test 19	T-H-S	C3	1500	6	3.2	186.51	4.69	84.1	153	55%
Test 19	T-H-S	C4	2000	12	3.2	248.68	3.13	17	153	11%
Test 21	T-H-R	C1	750	1	3.2	93.25	14.06	63.7	153	42%
Test 21	T-H-R	C2	775	1	3.2	96.36	14.53	68.5	153	45%
Test 21	T-H-R	C3	1500	4	3.2	186.51	7.03	120	153	78%
Test 21	T-H-R	C4	1500	4	3.2	186.51	7.03	123	153	80%
Test-22	T-H-R	C1	900	2	3.2	111.91	8.44	159	153	100%
Test-22	T-H-R	C2	925	2	3.2	115.01	8.67	164	153	100%
Test-22	T-H-R	C3	1000	2	3.2	124.34	9.38	146	153	95%
Test-22	T-H-R	C4	1050	2	3.2	130.56	9.84	131	153	86%
Test-23	T-L-S	C2	800	2	3.2	99.47	7.50	38.2	143	27%
Test-23	T-L-S	C3	800	3	3.2	99.47	5.00	0	143	0%
Test-23	T-L-S	C1	800	1.5	3.2	99.47	10.00	68.4	143	48%
Test-23	T-L-S	C4	800	4	3.2	99.47	3.75	0	143	0%
Test-24	T-L-R	C2	2000	12	3.2	248.68	3.13	0	143	0%
Test-24	T-L-R	C3	2000	10	3.2	248.68	3.75	41	143	29%
Test-24	T-L-R	C4	2000	8	3.2	248.68	4.69	64	143	45%
Test-25	T-L-R	C1	1500	8	3.2	186.51	3.52	28.5	143	20%
Test-25	T-L-R	C2	1000	6	3.2	124.34	3.13	0	143	0%
Test-25	T-L-R	C3	400	0.5	3.2	49.74	15.00	0	143	0%
Test-25	T-L-R	C4	350	3	3.2	43.52	2.19	0	143	0%

Table 3-5. Laser remelting parameters

3.4 MORPHOLOGY AND MICROSTRUCTURAL CHARACTERIZATION

3.4.1 Sample Preparation for Characterization

In order to characterize the coated structures, two different sample preparation processes were used: firstly, for the as-sprayed TBC coating without any remelting, samples were sectioned with a diamond cut-off wheel and then cold mounted and finally ground and polished. In these samples, sectioning the samples did not cause any significant damage to the microstructure of the coating. For the second set of preparation conditions which were used to prepare the laser melted samples, the coated and remelted samples were first sectioned into two pieces; one piece was mounted while the second piece remained untouched to do further surface tests. Since the remelting process makes the coating surface brittle, the coating starts to delaminate from the sample during normal sectioning, therefore, after the first sectioning step the sample half is cold mounted and sectioned once more prior to grinding. In this case, the remelted layer is supported by the mounting material during sectioning as well as during grinding and polishing.

3.4.1.1 Sectioning

A cut-off machine (Secotom-15, Struers, Canada) is used to cut the samples into pieces. Samples are fixed between the movable jaws of the cutting machine in the desired position. It is essential that cutting be done in a particular sample orientation. To reduce the potential for delamination in the coating, it is preferred to implement a compressive pressure on the coating surface, which means that the blade shall cut through the coating first and then head towards the substrate. Both cutting wheel speed (rpm) and feed rate could be adjusted in this regard. The cutting wheel speed was kept constant at 3000 rpm and a cutting feed rate of 0.01 mm/s was found to produce good quality cutting without any deviation from the straight line. A continuous flow of

water on the sample during the cutting process helped to keep the sample cool and aid the cutting process.

3.4.1.2 Cold-Mounting:

A mixture of resin and hardener with a 3 to 1(weight ratio) is prepared for the cold mounting process. Coated samples are placed precisely in the middle of a rubber mould so that the cross-section of the samples meet the near end of the mould. The moulds are filled with the resin and hardener mixture. During the stirring of the resin and hardener, some bubbles are created which were evacuated from the mixture as much as possible with a vacuum system (Cito Vac, Struers, Canada) which creates a vacuum under of 10 kPa for 10 minutes to remove the bubbles. After this step, the samples were removed from the machine and stored under the vacuum hood for twenty-four hours to cure the samples. Molded samples can be removed easily from the cups which have detachable bottoms.

3.4.1.3 Grinding and Polishing

The final step of sample preparation is reaching a surface condition acceptable to be observed under the microscope. In this regard, samples were placed through a series of grinding-polishing stages using an automated polishing machine (Tegramin-25, Struers, Canada). The machine's sample holder has the capacity for six pieces, but to grind and polish the samples symmetrically, either six or three samples shall be installed in each step. The grinding and polishing machine is programable based on the material used in each test. Also, both the head and platen of the machine are capable of rotating clockwise or vice versa. The best possible process started with grinding using the coarse abrasive silicon carbide (#320), followed by #500 and #800; after each step,

samples were removed from the machine and washed. Finally, during the polishing different polishing cloths with diamond abrasive (9, 3 and 1 μm) in water-soluble oil was used as shown in Table 3-5. These removed any deformation resulting from grinding, reaching a mirror-like surface.

Row	*Step*	*Code*	*Time (min)*	*Lubricant*
1	Grinding	#320	03:00	Water
2	Grinding	#500	01:00	Water
3	Grinding	#800	01:30	Water
4	Polishing	Plan	06:00	DiaDuo- 9 μm
5	Cleaning	-----	00:30	Water
6	Polishing	Dac	05:00	DiaDuo- 3 μm
7	Cleaning	-----	00:30	Water
8	Polishing	Nap	02:00	DiaDuo- 1 μm
9	Cleaning	-----	00:30	Water
10	Polishing	Chem	02:30	OP-S
11	Cleaning	-----	00:30	Water

Table 3-6. Grinding and polishing parameters

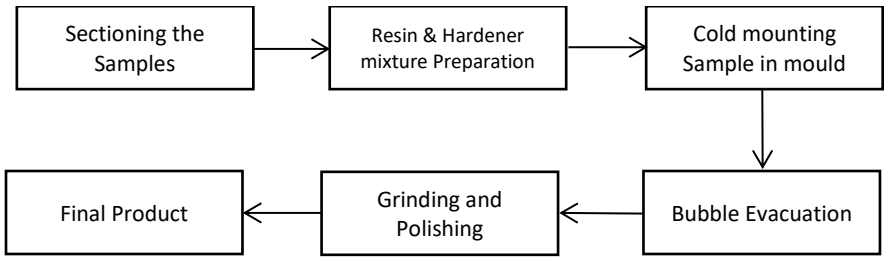

Figure 3-7. Sample preparation flow chart for SPS samples

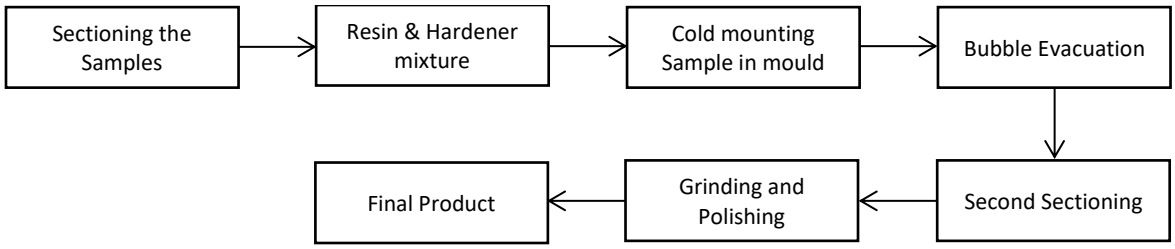

Figure 3-8.Sample preparation flow chart for laser remelted samples

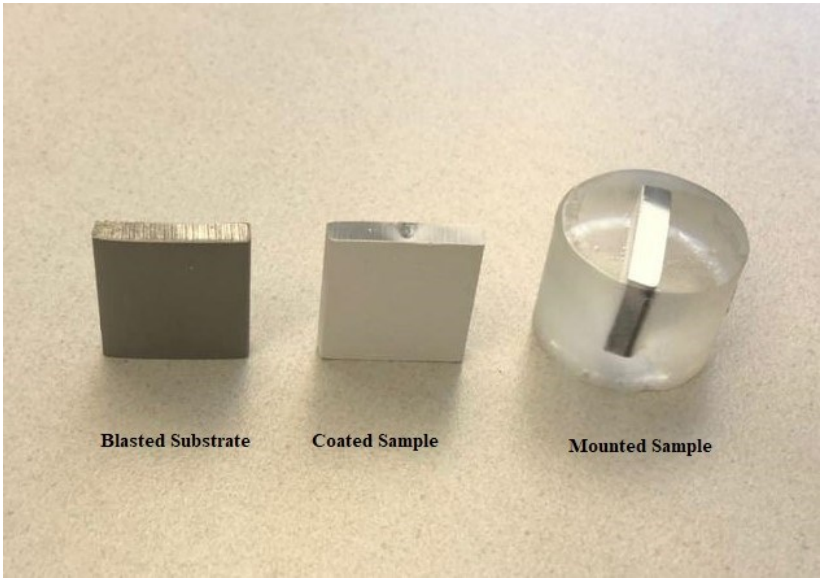

Figure 3-9. Final samples

3.4.2 Morphology and Characterization Equipment

A Scanning Electron Microscope (SEM, Hitachi, S-3400N) was used in order to perform SEM on the cross-section of the coated samples. Samples were fixed with a carbon film to prevent charging during examination. Since there was a large number of samples, preliminary observations were carried out with an Olympus GX51 optical microscope to evaluate the cross-section conditions. Moreover, to view the top surface state and obtain a 3D topography image, a 3-D Confocal Laser Scanning Microscope (CLSM) (LEXT-OLS4000, Olympus Corporation, Japan) was used. Finally, to measure the porosity and thicknesses of the melted layer, image analysis software (ImageJ Fiji) was used on the obtained structures.

4 RESULTS AND DISCUSSIONS

Using suspension plasma spray in order to produce thermal barrier coatings has the potential to enhance the properties of the coating microstructure in comparison with other methods [11], [28], [31], [63]. In this research, laser remelting was used to study the probability of improving on these properties. SPS has a unique capability of producing different porous and columnar microstructures with a potentially longer service lifetime and, at the same time, a lower thermal conductivity. However attack by molten CMAS (CaO-MgO-Al_2O_3-SiO_2) can preferentially dissolve the boundaries of these microstructures, which is harmful to the coating structure [64]. This thesis aims to utilize the laser to modify the coating surface properties such as surface roughness, sealing of open porosity, and generating a controlled, segmented crack network using the columnar SPS coating microstructure to reduce the penetration rate.

In this chapter, the comparison between the microstructure of the coatings obtained by in-house and commercial suspensions will be reviewed. It will be followed by the results obtained from surface remelting of the different coatings.

4.1 IN-HOUSE AND COMMERCIAL COATINGS

The influences of the suspension characteristics on coating microstructure are studied by using two different suspensions. As was mentioned, in-house and commercial suspensions were used to deposit coatings on the substrate. In this work, a 25% YSZ suspension was sprayed into plasma jet; for further details, please refer to Table 3.3 The microstructures of the coatings

generated with these two suspensions are shown in Figure 4-1. In this figure, all pictures on the left-hand side (LHS) are sprayed onto substrates with a surface roughness of 1.6 μm while those on the right-hand side (RHS) demonstrate coatings applied on substrates with roughness of 4.5 μm. Figure 4-1. a, b, c, and d are generated from the commercial suspension (T-B) and the remainder are prepared with the in-house (I-H) suspension. Conditions a & b were spayed with 45 ml/min feed rate and a robot speed of 1 mm/s and these conditions are referred to as ***SPS 1*** from now on, while conditions c & d were sprayed with a feed rate of 30 ml/min and a robot speed of 1.5 mm/s, which will be called ***SPS 2***. In Figure 4-1, the micrographs (e, f, g, and h) were generated from in-house suspensions sprayed towards the substrate. Samples (e) and (f) were sprayed under the SPS 1 conditions, and (g) and (h) under SPS2 to compare the commercial and in-house suspension characteristics. As is clear in Figure 4-1, using the commercial suspension has a significant influence on the coating microstructure and resulted in an identifiable columnar structure with a porous coating under these spray conditions.

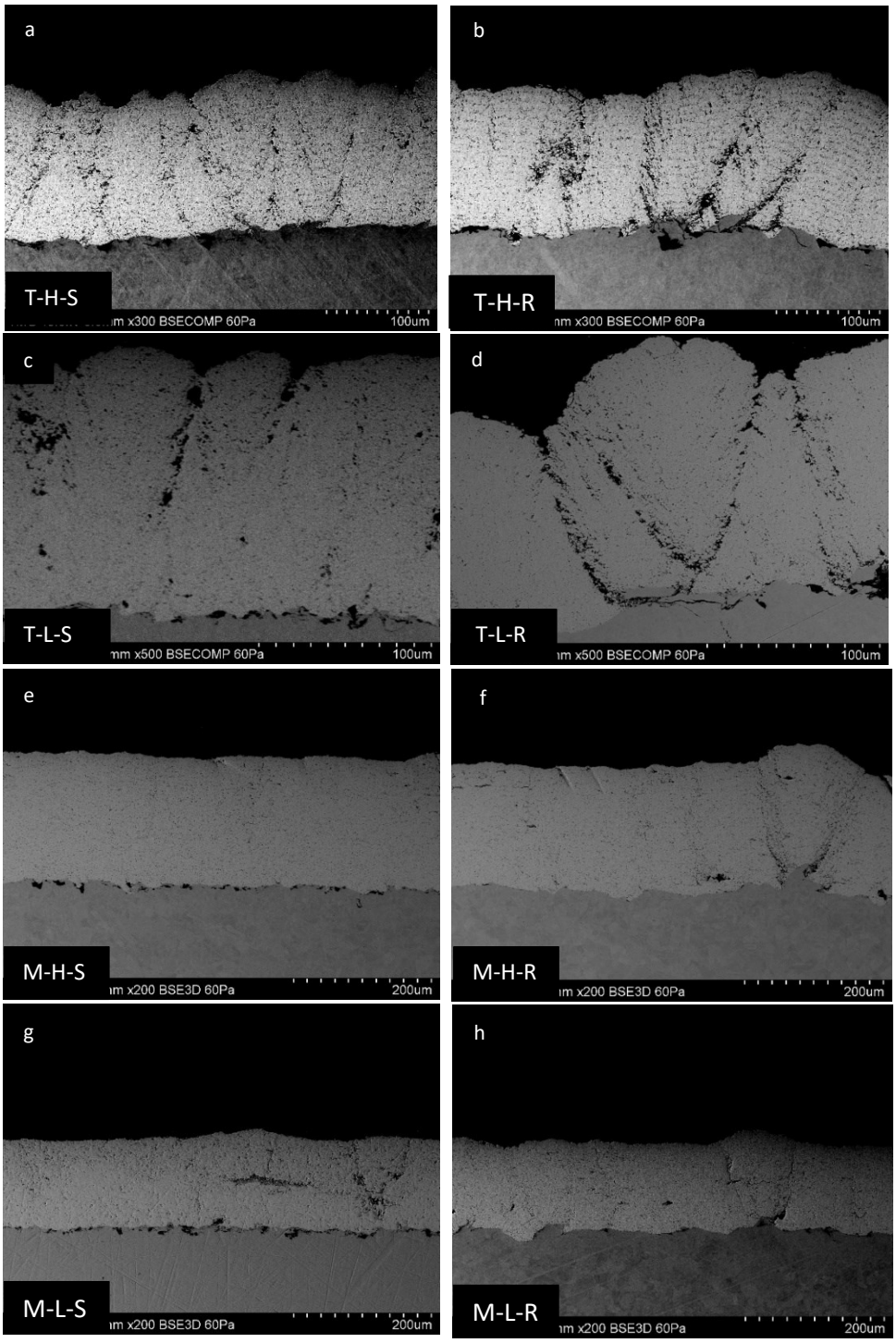

Figure 4-1. SEM Images of coating cross sections from commercial (a,b, c, d) and in-house (e,f,g,h) suspensions. Substrate roughness of 1.6 µm (a, c, e & g) and 4.5 µm (b,d, f & h)

The column formation in SPS coatings depends on the path of the nanoparticles in the plasma just before impact with the substrate and this is called the shadow effect as shown in Figure

4-2. The method to calculate the microstructure crack density utilized in this study was that proposed by Ganvir et al. [18]. In this method, a horizontal line is drawn in the middle of the coating, and the number of vertical cracks (or column thicknesses) which intersect these lines will be counted. The number obtained by this method is divided by the length of the line and will give us crack density per millimeter (or column thickness). Upon reviewing the microstructures of the two coatings, they show that the crack density in T-H-S was 19.6 ± 2 (cracks/mm) whilst for T-H-R it is 11.09± 3 (cracks/mm) thus increasing the substrate roughness reduced the crack density. Consequently, the average column thickness was lower in T-H-S in comparison with T-H-R, with an average column size in T-H-S of 69.1±13µm and 91.2±12 µm for the rough substrate (T-H-R). For these cases, in order to lower the speed of particles at the time of impact (and lower Stokes number) [68], a spray distance of 100 mm was used. Based on Figure 4-2, T-H-S

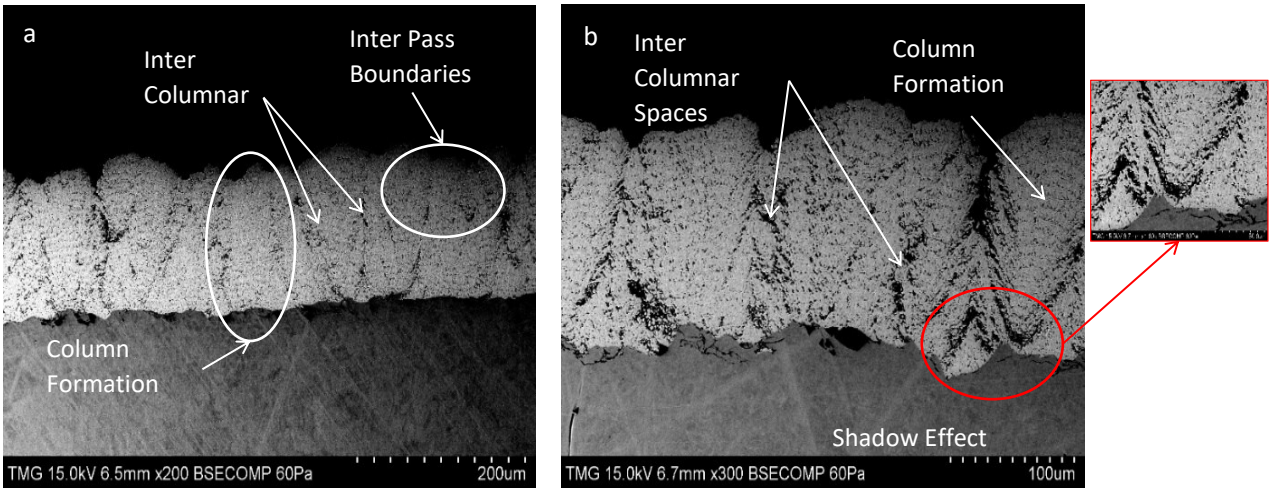

Figure 4-2. Effect of surface roughness on column formation (a) Sample T-H-S with roughness 1.6 µm and (b) Sample T-H-Rwith roughness 4.5 µm

which has the lower roughness, generates a coating structure with lower porosity in comparison with T-H-R. The porosity increases from 14% to 19% which is significant in two major ways [30]: firstly on the lifetime of the coating and secondly on the thermal conductivity of the coatings, since the higher amount of porosity acts as insulation in the coating structure, although thermal conductivity is affected by vertical cracks and intercolumnar distances as well [65]. Samples T-L-S and T-L-R were sprayed under the same conditions on the two substrates types T-L-S -in the same way as already explained for T-H.

The crack density for these samples was also measured: for T-L-S it was 18.35 cracks/mm and for T-L-R it was 10.35 cracks/mm. The column width in T-L-R is 58.1 μm compared to 42.4 μm in T-L-S.

The results related to tests T-H and T-S samples are summarized in Table 4-1. Based on the information presented in Figure 4-4, decreasing the feed rate caused a lower amount of suspension to be injected into the plasma plume. Therefore, a lower amount of material receives the same amount of energy. This energy caused a full melting of the suspension and fully melted particles impacted with the substrate. This results in the creation of a structure with lower porosity in

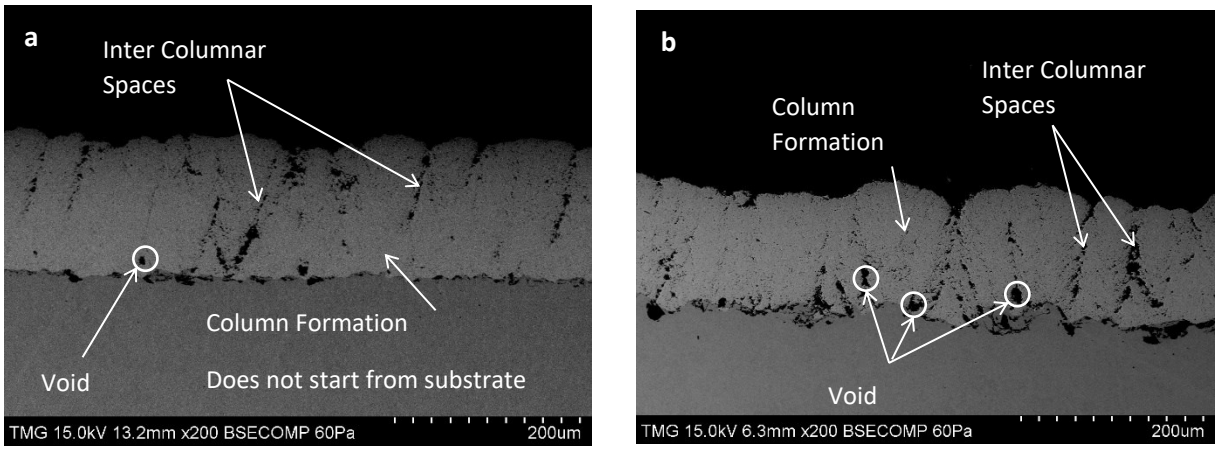

Figure 4-3. Effect of roughness in column formation (a) T-L-S (b) T-L-R

comparison with the higher feed rate samples. Another point is the creation of inter-pass boundaries in the T-H-S and T-H-R tests, which is the result of the high deposition rate and impact of unmelted and/or partially melted particles on the substrate; on the other hand, increasing the lateral robot head speed increases the turbulence of the particles and makes columns grow in different directions which increases the creation of voids in the structure.

Sample	*Substrate Roughness Ra (µm)*	*Feed rate (ml/min)*	*Crack Density (cracks/mm)*	*Column Size (µm)*	*Porosity %*	*Coating Thickness*
T-H-S	1.6	45	20±2	69±12	15	155
T-H-R	4.5	45	11±2	92±13	19	155
T-L-S	1.6	30	18±1	42±11	11	143
T-L-R	4.5	30	10±3	58±13	14	143

Table 4-1. Microstructure characterization and properties

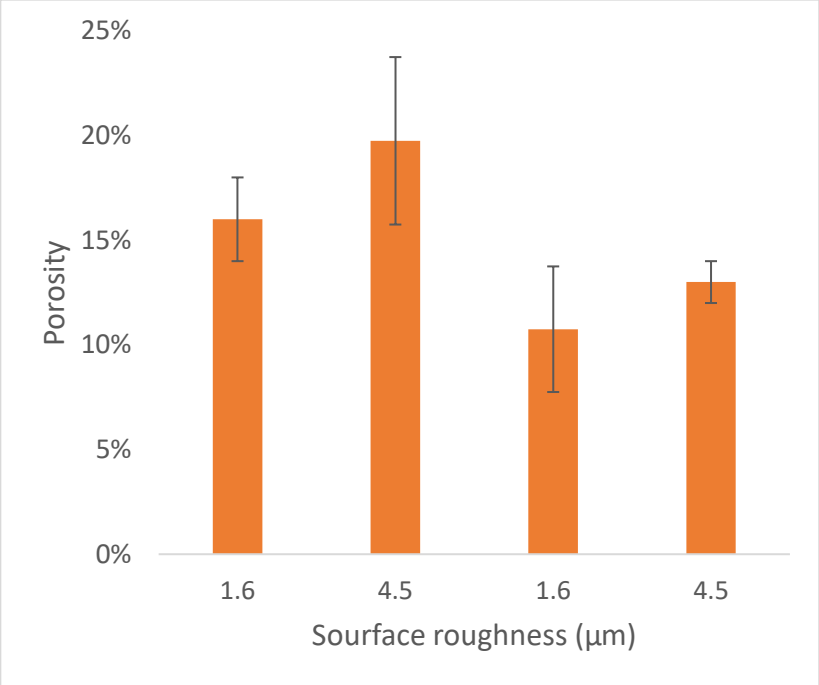

Figure 4-4. Porosity percentage of columnar structure in T-H-S, T-H-R, T-L-S & T-L-R.

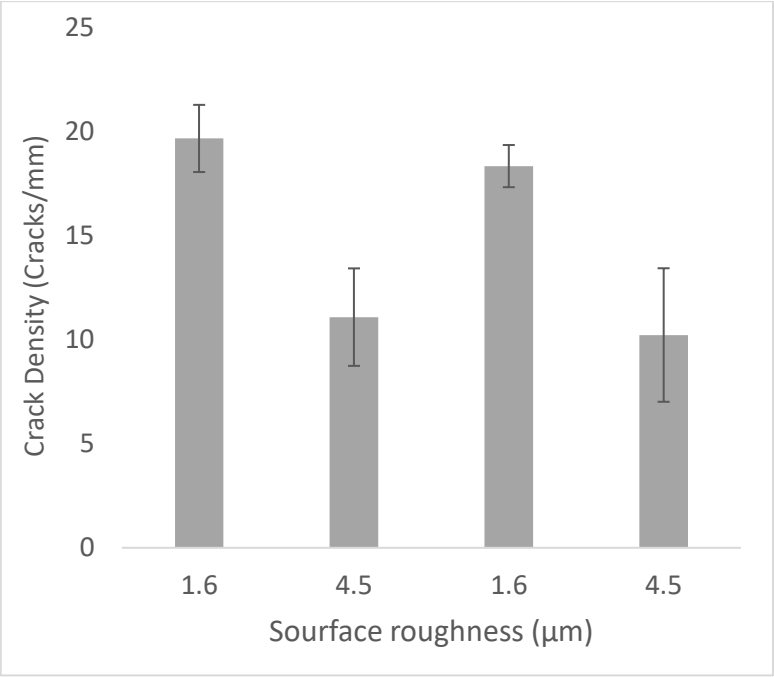

Figure 4-5. Crack density comparison of T-H-S, T-H-R, T-L-S & T-L-R.

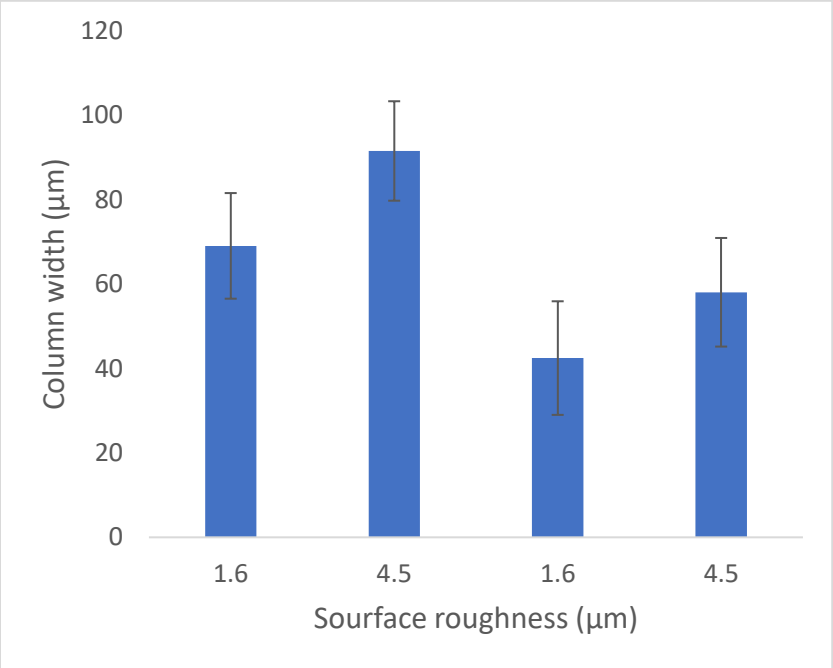

Figure 4-6. Column size comparison of T-H-S, T-H-R, T-L-S & T-L-R.

Therefore, it can be confirmed that increased substrate roughness results in increased column width. In addition, the porosity of the coatings on the rougher substrate T-L-R (14% porosity) was again higher than on the less rough substrate T-L-S (11%).

As was previously stated in Table 3-2, samples M-H-S and M-H-R were sprayed with the in-house suspension but with the same conditions as T-H and T-L. This decision was based on the knowledge that the average particle size $D_v(50)$ of both suspensions were in the same range.

Based on the image analysis of the micrographs of the M-H-S sample (R_a = 1.63 µm) the porosity was measured as 4%, which is much lower in comparison to the commercial suspension sample with similar conditions, T-H-S. For M-H-R (R_a = 4.5 µm) the increased surface roughness raised the porosity slightly to 6% which is still much lower than the amount achieved with the commercial suspension. As the final test, M-L-S and M-L-R samples are sprayed under SPS2 conditions, (a

feed rate of 30 ml/min and a robot head speed of 1.5 mm/s) with the in-house suspension and as a result of complete melting of the particles and their impact on the substrate, a dense structure is obtained in comparison with the previous samples. Despite the increased substrate roughness, the microstructure was not significantly improved.

4.2 CHARACTERISTICS OF REMELTED COATINGS

The coating microstructure morphology and the remelted layer surface were analyzed using optical and scanning electron microscopy (SEM). Cross-section planes, perpendicular to the laser beam travel direction, were prepared to analyze different parameters on the remelted layer microstructures.

4.2.1 Cross Section Characterization

The microstructures of the coatings exposed to the laser are influenced by several parameters. Before going any further, to better understand the laser behavior on the YSZ coating the power density and energy density of the beam are calculated based on the experimental conditions and are considered as two significant parameters in our results [51].

$$P_d = \frac{4P_{out}}{\pi d^2} \qquad \text{Eqn-1}$$

$$E_d = \frac{P_{out}}{Vd} \qquad \text{Eqn-2}$$

In the above formula P_d is the power density in $(^{MW}/_{m^2})$ and E_d is the energy density in $(^{J}/_{mm^2})$, $P_{out}$is the laser output power in Watts, d is the laser spot diameter, and V is the laser scanning speed. To study the effect of the laser output power, various power ranges were applied

on different surfaces. The highest power utilized is 2000 Watts, and the lowest was 350 Watts. Power density, which is laser beam power per unit area, directly relates to laser output power due to Eqn-1 and is independent of scanning speed. Energy density is the energy applied to the surface area, based on Eqn-2 and has a direct relation with output power and has an inverse relation with scanning speed. Based on the tests, in order to avoid burning the substrate, the relation between scanning speed and output power should be considered simultaneously.

In this regard, T-H-S samples were remelted under four conditions (C1 through C4) and named as Test-19 and the results are presented in Figure 4-7.

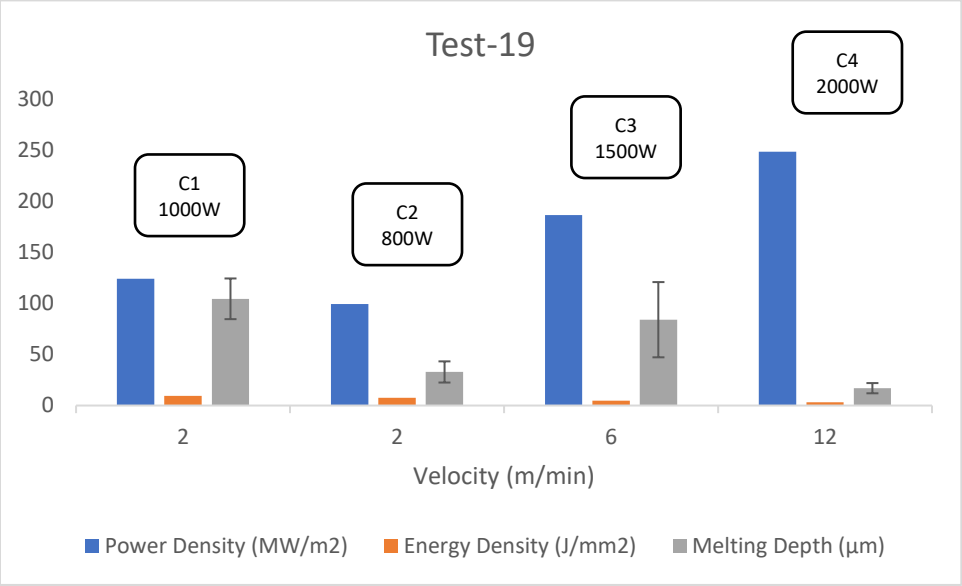

Figure 4-7. Test-19 power density, energy density, and melting depth for C1 to C4 on T-H-S

In this test, all four conditions result in surface remelting. Under the first condition (in which, based on our previous experiences on non-columnar structures, the power of the laser was set to 1000 W with a speed of 2 m/min), 83% of the TBC layer or around 104 µm was melted (Figure 4-8 (a)), which is not desirable as too much of the layer is affected. By decreasing power by 20% to 800 W at the same speed, the power density and energy density both decreased which

results in a reduction in melting depth to 33% (b) which was 32.9 μm. The problem with this condition was nonuniform melting. In order to overcome this problem and reduce the melting depth, higher powers with higher speeds were tested: power density was increased by 46% and actual output power reached 1500 W and the scanning speed was increased to 6 m/min. As a result, the energy density was reduced as shown in Figure 4-8 (c) but some voids were generated in the remelted layers as a result of fast solidification. Air could not escape in time from the melted layers and was trapped in that layer. Finally, the power was increased to its maximum, 2000 W, which is doubled in comparison with condition 1, and the speed increased to 12 m/min. The result was remelting to a depth of ≈ 17 μm which was 11% of the TBC thickness. This was a very satisfactory depth but the problem with this set of parameters was the inconsistency of the melted layer.

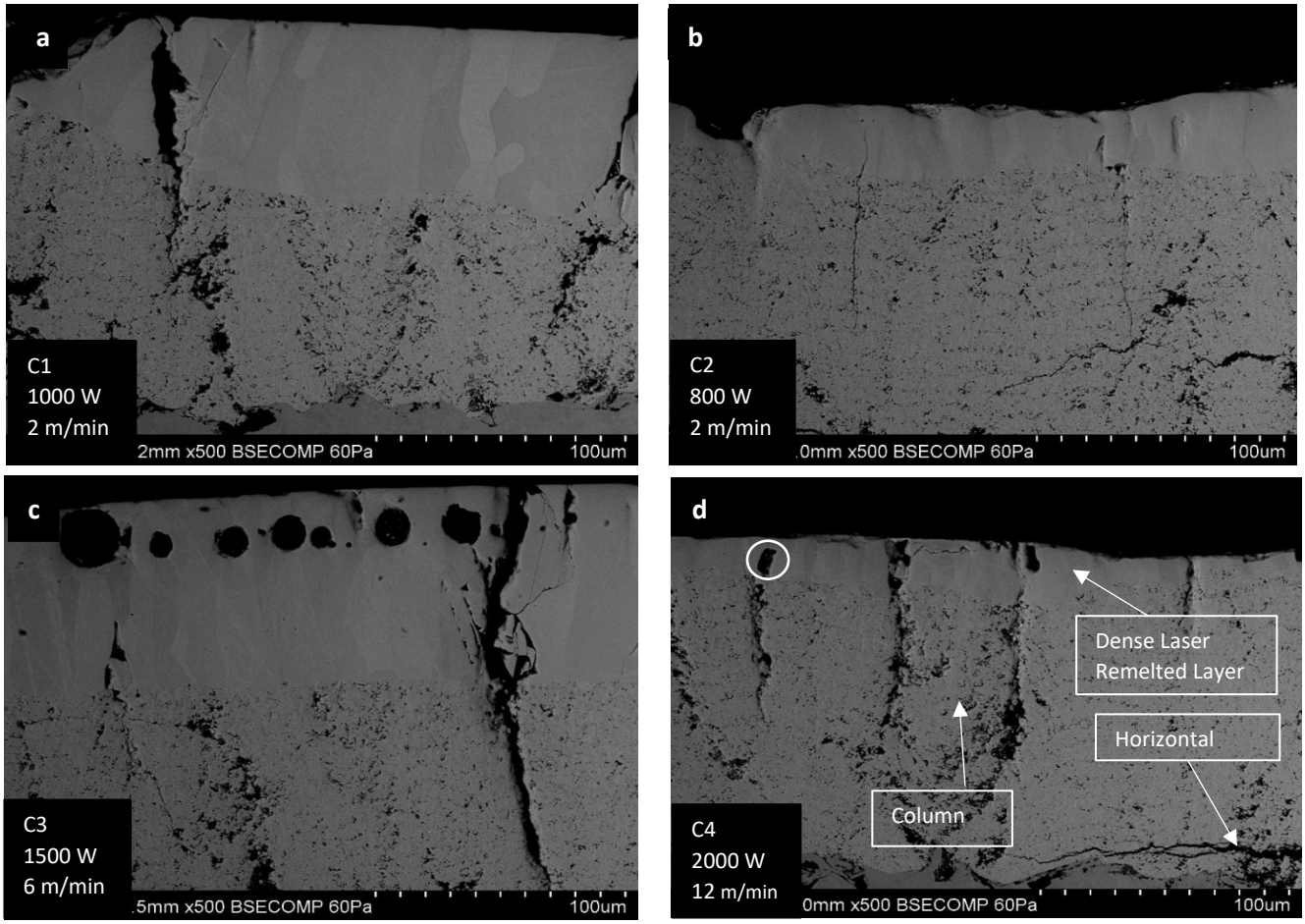

Figure 4-8. SEM Image from cross section, Test 19, T-H-S (a) Condition 1 (b) Condition 2 (c) Condition 3 (d) Condition 4

As we can see in Figure 4-9, in Test 21, which is carried out on T-H-R sprayed samples, the influence of moderate to high power and low scanning speed is observed. Based on Test-19, a high-power beam with high speed resulted in remelting of a thin layer of the TBC coating on top of the columnar structure, but the high scanning speed of the laser produced a nonuniform melted layer.

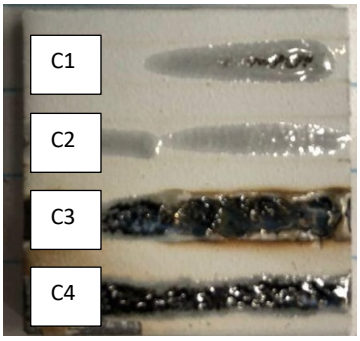

Figure 4-9. Test 21 T-H-R Surface condition

To avoid such conditions and obtain more uniform melting across all the surface, a low scanning speed with moderate power was tested. Initially, the speed of the robot head traverse was reduced to 1 m/min and laser powers of 600 W and 650 W were tried but the substrate surface was not affected. By increasing the power 25% to 750 W (Figure 4-9 C1), the energy density rose to 14.06 ($^{J}/_{mm^2}$), which was almost five times higher than that of Condition 4 of Test-19 which had resulted in melting through 11% of the layer thickness. This new condition increased the melting to 42% of layer thickness, which is an excessive amount of melting, but in this case, melting uniformity increased significantly. In the second condition, power was slightly increased by 3% to improve the melting quality, hence the melting depth increased to 63 µm (45%), but the uniformity of the remelted layer improved considerably (Figure 4-9 C2). During the last conditions, C3 &4, both scanning speed and power were increased, such that the power density increased by 50% and rose to 186.5 ($^{MW}/_{m^2}$), and energy density decreased by 50% to 7.03 ($^{J}/_{mm^2}$). Still, in this case, the laser burned the coating layer totally and heated the substrate. Therefore, it can be said that there is not a linear relation between power and scanning speed and melting depth.

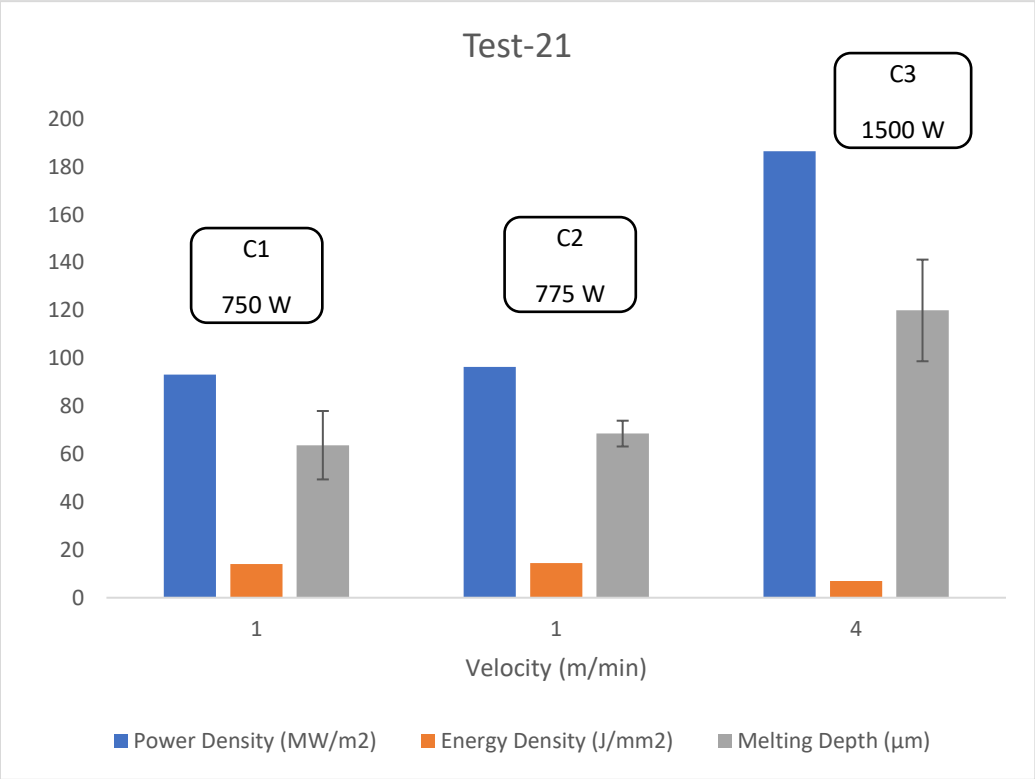

Figure 4-10. Test-21 T-H-R power density, energy density and melting depth for C1 to C3

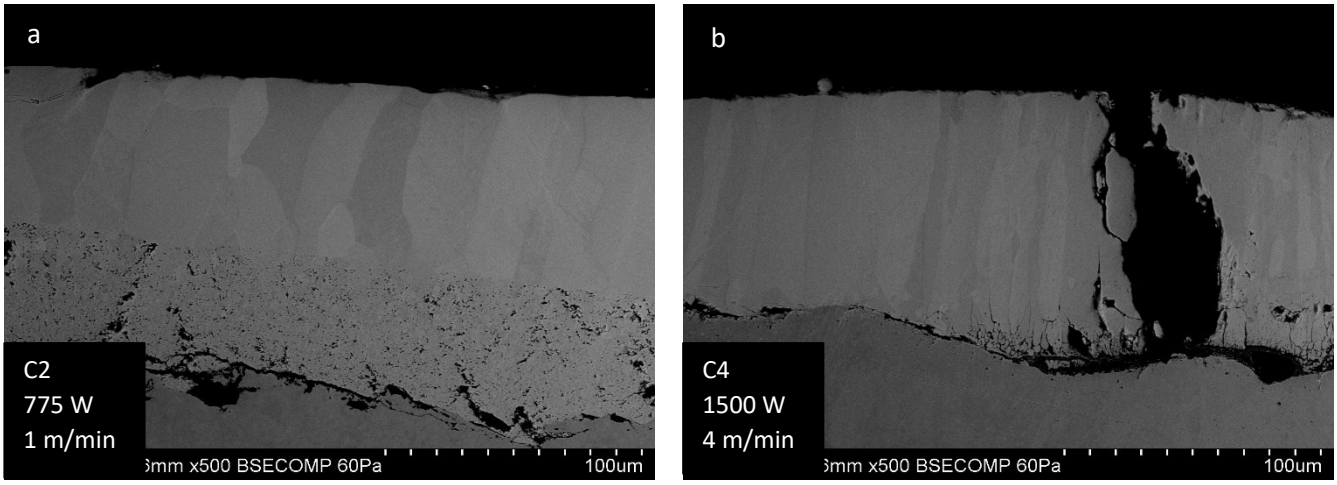

Figure 4-11. SEM image cross section Test 21 T-H-R (a) Condition 2, uniform melting all over the surface (b) Condition 4, high power and scanning speed burned the whole layer and substrate

During Test-22, to improve on the conditions of Test-21 in which remelting started, both scanning speed and power were increased. Scanning speed was increased by 100% to 2 m/min compared to Test 21 and the power was increased to 900 W and 925 W. As shown in Figure 4-12 a mixture of un-melted, melted and burnt layers are produced in these cases. Finally, in the last condition C4 of this test, the power was increased by 37% and reached to 1025 W and compared to Test-21 C1, and in this case, despite a high melting thickness of 80% the remelting uniformity improved.

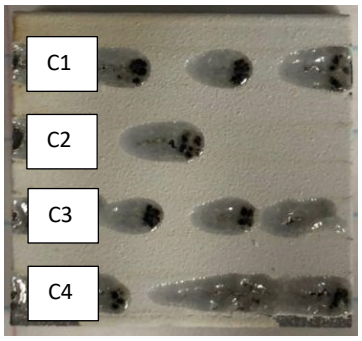

Figure 4-12. Test 22, T-H-R surface condition

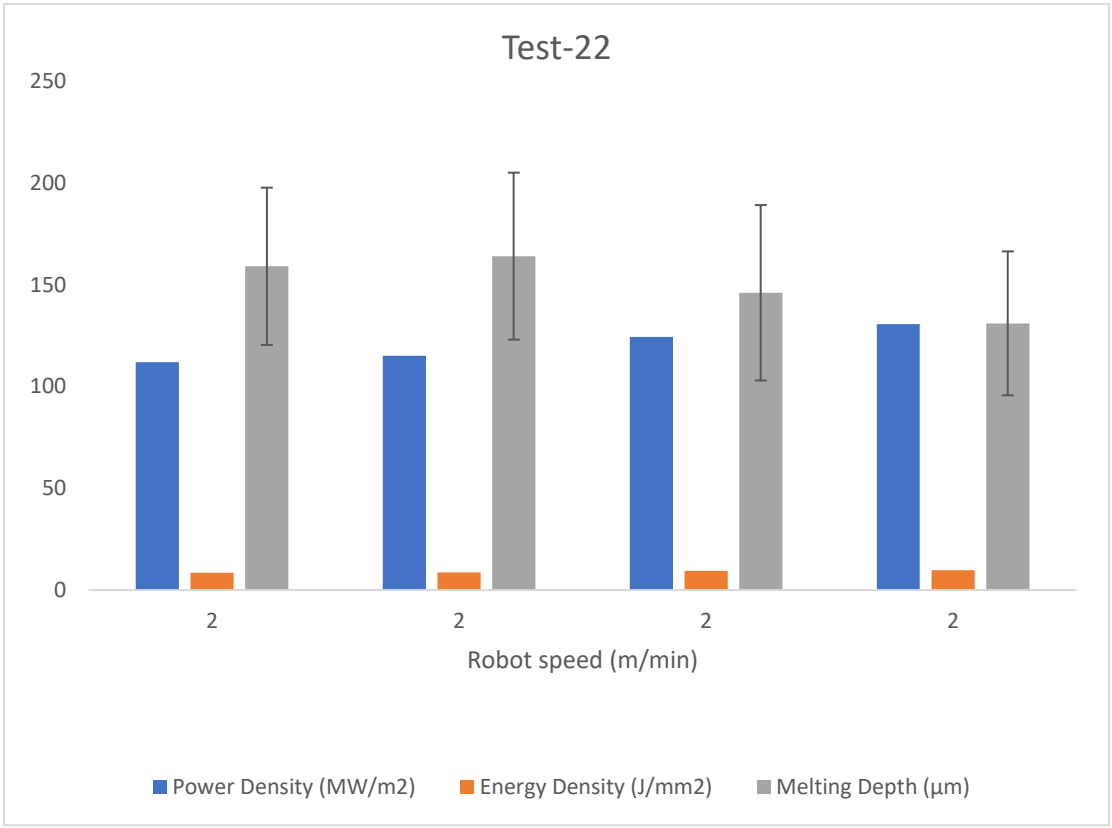

Figure 4-13.Test-22, T-H-R power density, energy density and melting depth for C1 to C4

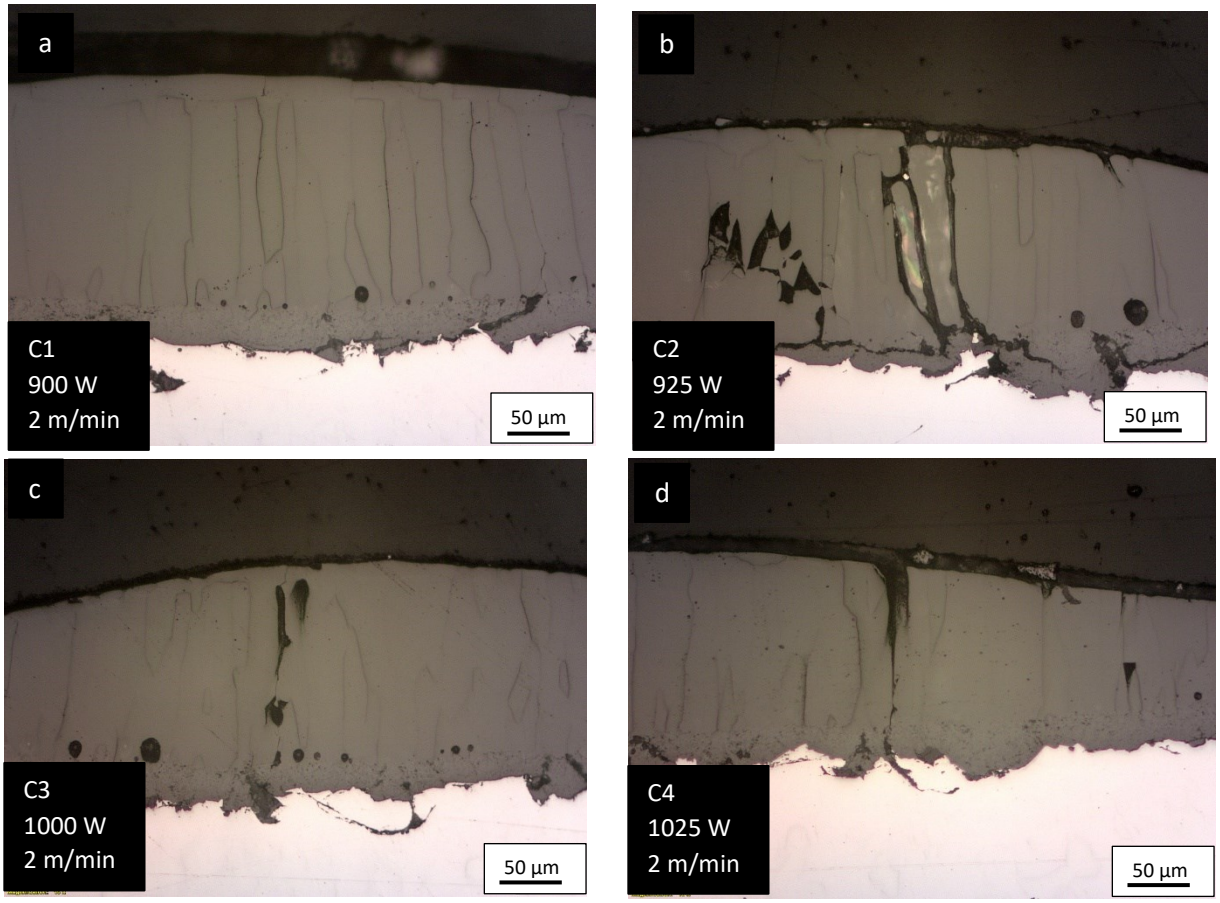

Figure 4-15. Optical microscope image of cross section pictures of Test 22- , T-H-R (a) Condition 1 (b) Condition 2 (c) Condition 3 (d) Condition 4

In Tests 23 and 24, the power density was fixed in order to study the effect of scanning speed and consequently energy density on remelting and thus the relation between power density and energy density. During Test-23, (800 W) the scanning speed is varied from 1.5 m/min to 4 m/min. With a fixed power density of 99.47 ($^{MW}/_{m^2}$), different energy densities were applied on the substrate. Using a speed of 2 m/min, resulted in 7.5 ($^{J}/_{mm^2}$) of energy density, which gave non-uniform melting on the laser path, and the melting depth in those areas which melted was 38.2 µm, which was 27% of the TBC thickness. This varying of the scanning speed under the same power confirmed Test-19, condition C2. Based on this experience, the scanning speed was

increased to 3 m/min. This increase caused a 50% reduction in energy density, and the laser treated layer changed from white to a yellow colour. However, the surface was not melted. At the time of the experiment, this color contrast caused us to believe we have some remelting of a very thin layer hence to increase the amount of melting and increase the uniformity of the remelted layer, the scanning speed was reduced to 1.5 m/min. This caused more uniformity of melting than the C1 condition. Unfortunately, the melting depth increased considerably to 68.4 µm, (or 48% of the layer thickness) which is not desirable in our case.

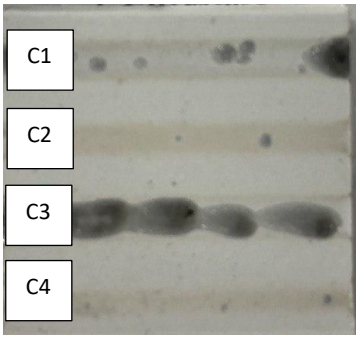

Figure 4-16. Test 23 T-L-S surface condition

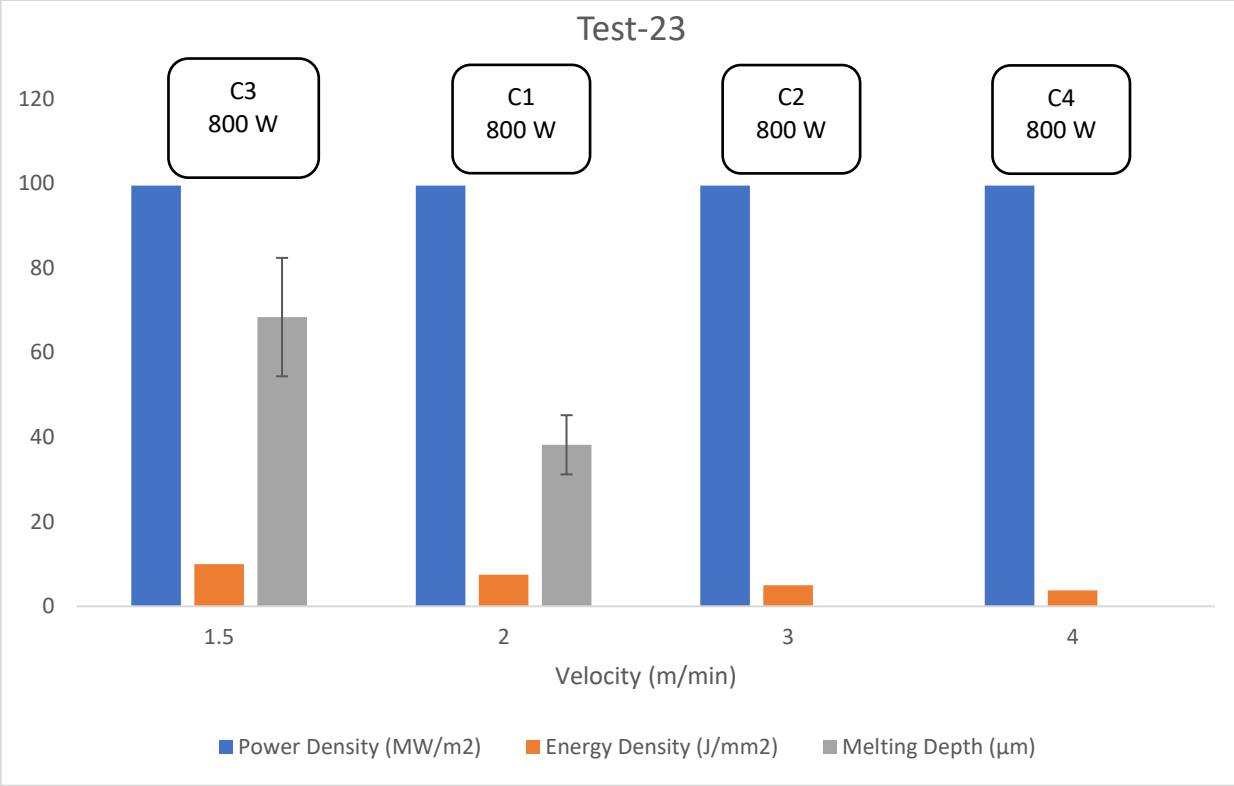

Figure 4-17. Test-23, T-L-S, power density, energy density and melting depth for C1 to C4

Finally, based on the change in the surface color to deep yellow (Figure 4-16 C2), the speed was increased to 4 m/min which gave a considerable reduction in energy density and no melting was observed.

Based on the results obtained in Test 19-C4 with a scanning speed of 12 m/min and power of 2000 W, these conditions were considered as the starting point for Test 24 parameters. In Test-24, unfortunately, the first condition (C1) was not usable since some technical issues came up during the test, hence, for the second condition (Test 24-C2), 2000 W of power and 12 m/min scan speed were set as the main conditions. As shown in Figure 4-18 C2 the color of the affected area changed from white to yellow again, but unlike Test-19, it did not result in melting. This could be a result of using a denser TBC coat in this case or nonuniform melting due to the higher speed in this test. In order to improve the results, the scanning speed was decreased to 10 m/min in C3, and

the energy density increased slightly from 3.13 to 3.75 ($^{J}/_{mm^2}$) . Still, since the power density is considerably high at 248.68 ($^{MW}/_{m^2}$), it caused melting to a depth of round 41 µm which was 29% of the coating thickness. Lastly, for condition C4, the scanning speed was decreased slightly to 8 m/min aiming to make the melting uniform, and the energy density was increased to 4.69 ($^{J}/_{mm^2}$). The melting increased to 45% of the coating thickness: a depth of ~ 64 µm. The information is summarized in Figure 4-19.

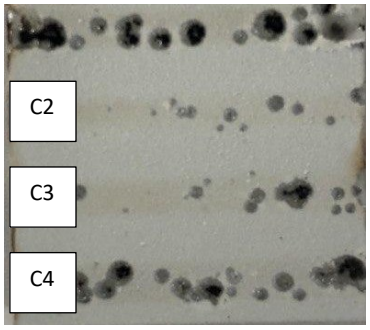

Figure 4-18. Test 24 T-L-R surface condition

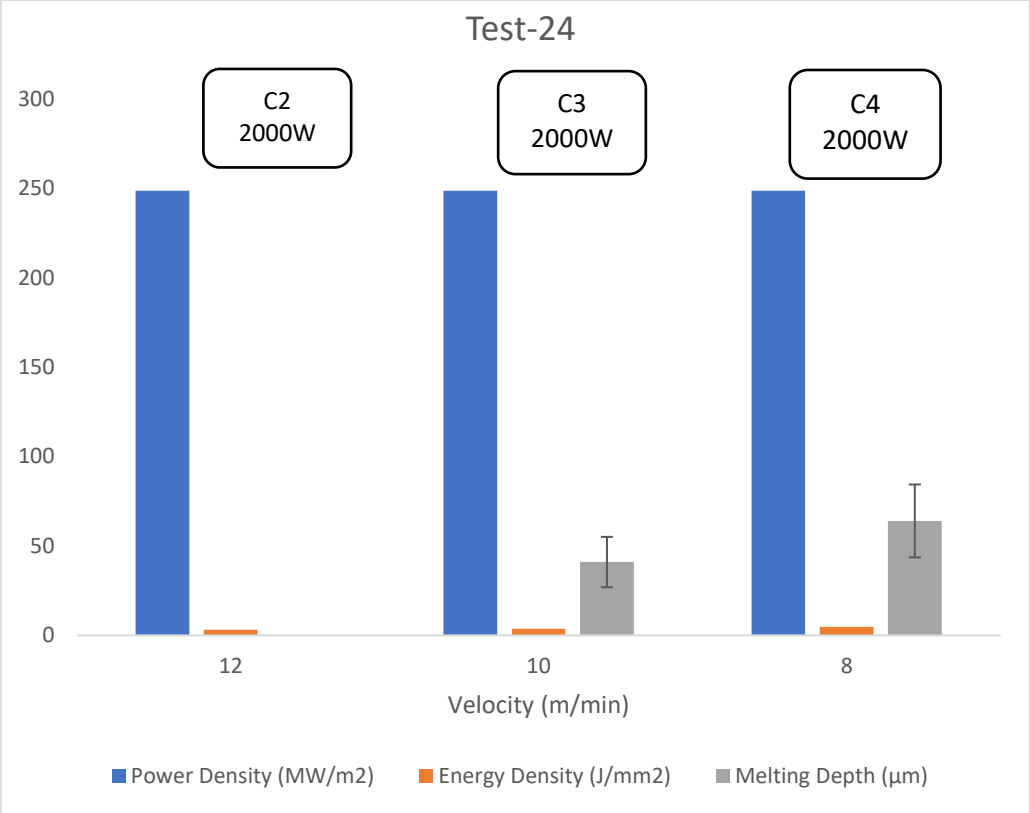

Figure 4-19. Test-24 on T-L-S, power density, energy density and melting depth for C2 to C4

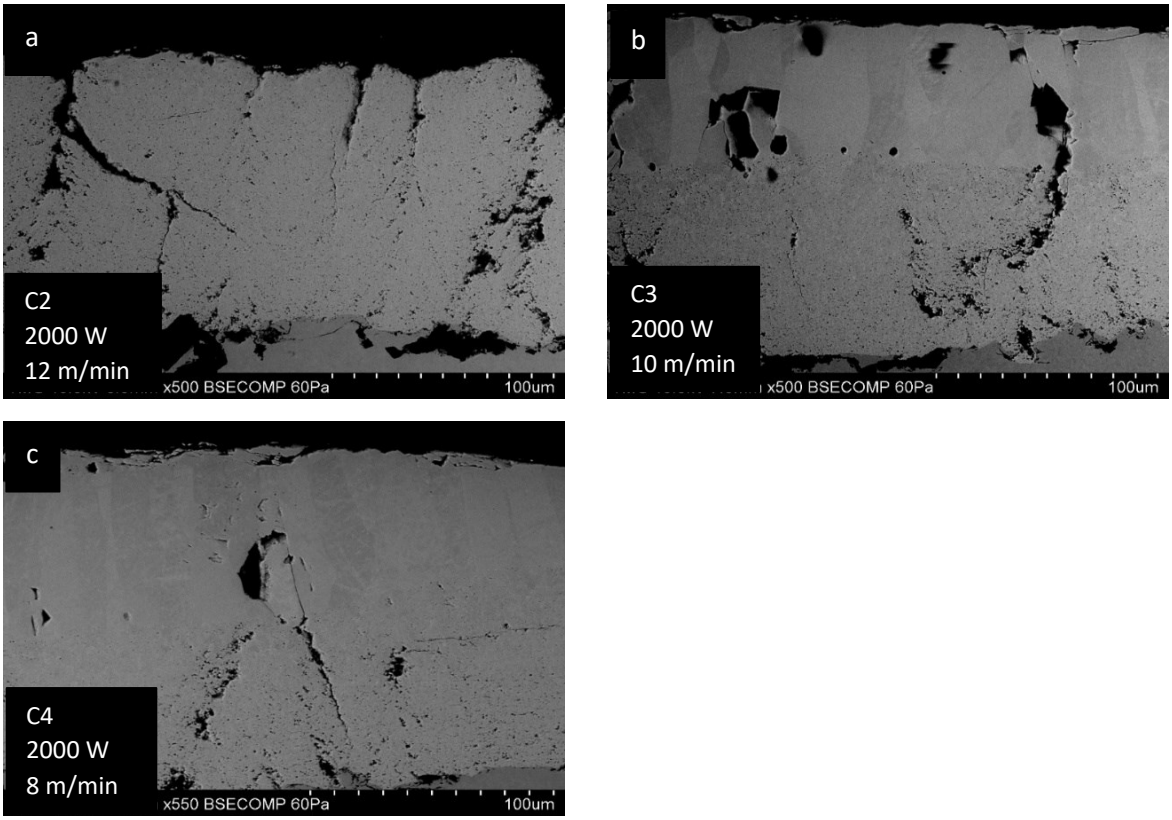

Figure 4-20. SEM image cross section Test 24- T-L-R (a) Condition 2 (b) Condition 3 (c) Condition 4

Finally, during Test-25, two main conditions were considered due to previous results: C1 was set at 1500 W power and a high scanning speed of 8 m/min and C3 was set at 400 W power and a low scanning speed of 0.5 m/min. These different parameters gave very different values of energy density. For C1, the first condition, the 1500 W power gives a power density of 186.51 ($^{MW}/_{m^2}$) and an energy density of 3.52 ($^{J}/_{mm^2}$) . This amount of energy caused melting to a depth of 28.5 µm, (20% of the coating thickness). By decreasing power from 1500 W to 1000 W and decreasing scanning speed from 8 m/min to 6 m/min in C2, the energy density decreased from 3.2 to 3.13 ($^{J}/_{mm^2}$) however no melting was obtained.

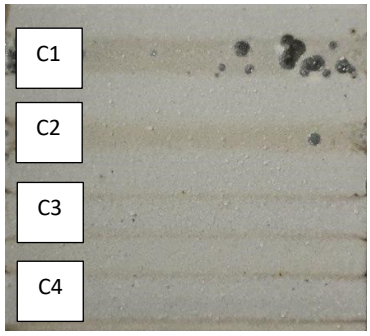

Figure 4-21. Test 25 T-L-R surface condition

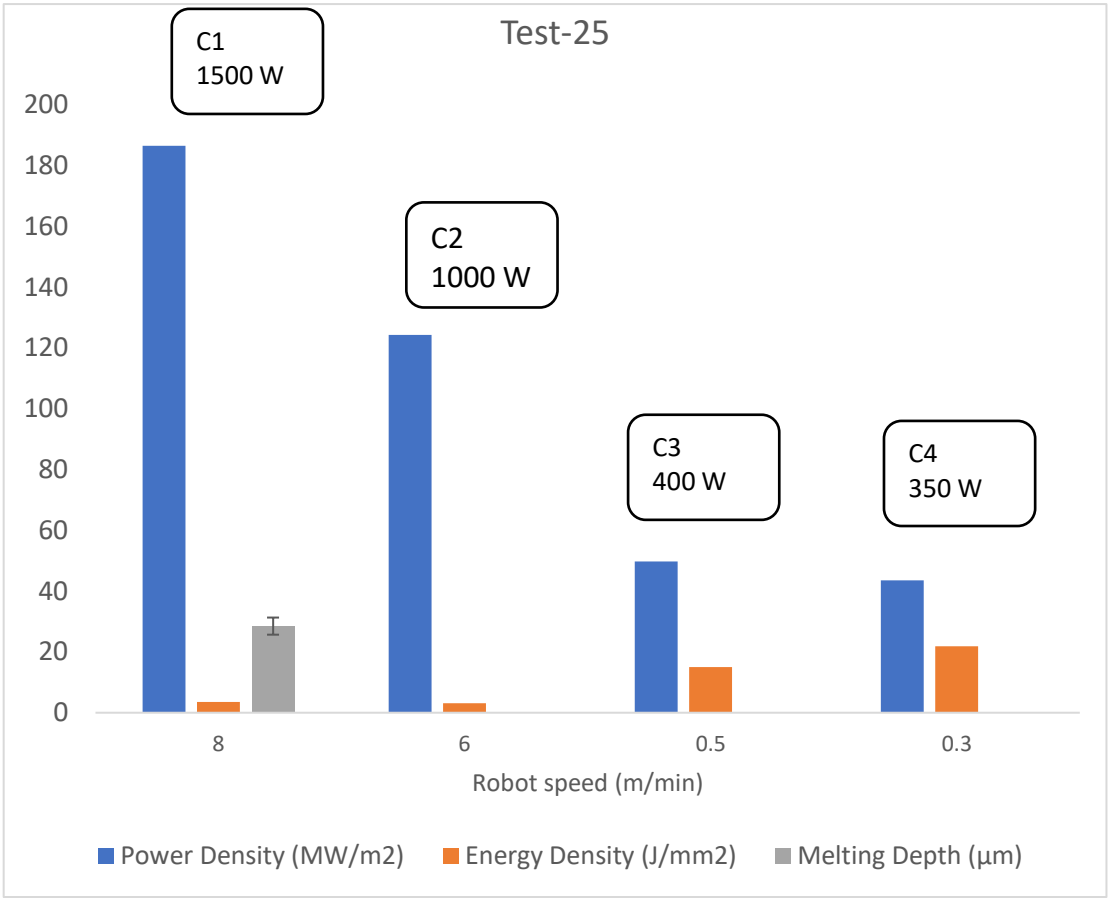

Figure 4-22. Test-25, T-L-R power density, energy density and melting depth for C1 to C4

For C3, by decreasing the scanning speed considerably to 0.5 m/min despite using a lower laser power, the energy density increased five times that of the first condition, C1 to 15 $\left(J/_{mm^2}\right)$. Despite having no melting in this area (C3), the surface was affected with heat, and sintering

occurred in this area (Figure 4-23 b, c). In order to improve the condition of C3, during the last condition (C4) the scanning speed was decreased to 0.3 m/min; hence the energy density increased from 3.52 in C1 to 21.88 $\left(J/_{mm^2}\right)$ in C4. To avoid any damage, the laser output power was set to 350 W in C4. In this case the power density decreased to 43.53 $\left(MW/_{m^2}\right)$. The result of this test is a uniform laser-affected zone but with no melting. The result of this Test-25 demonstrates that with the use of low scanning speeds, the uniformity of the laser affected zone will be considerably higher in comparison to high scanning speeds.

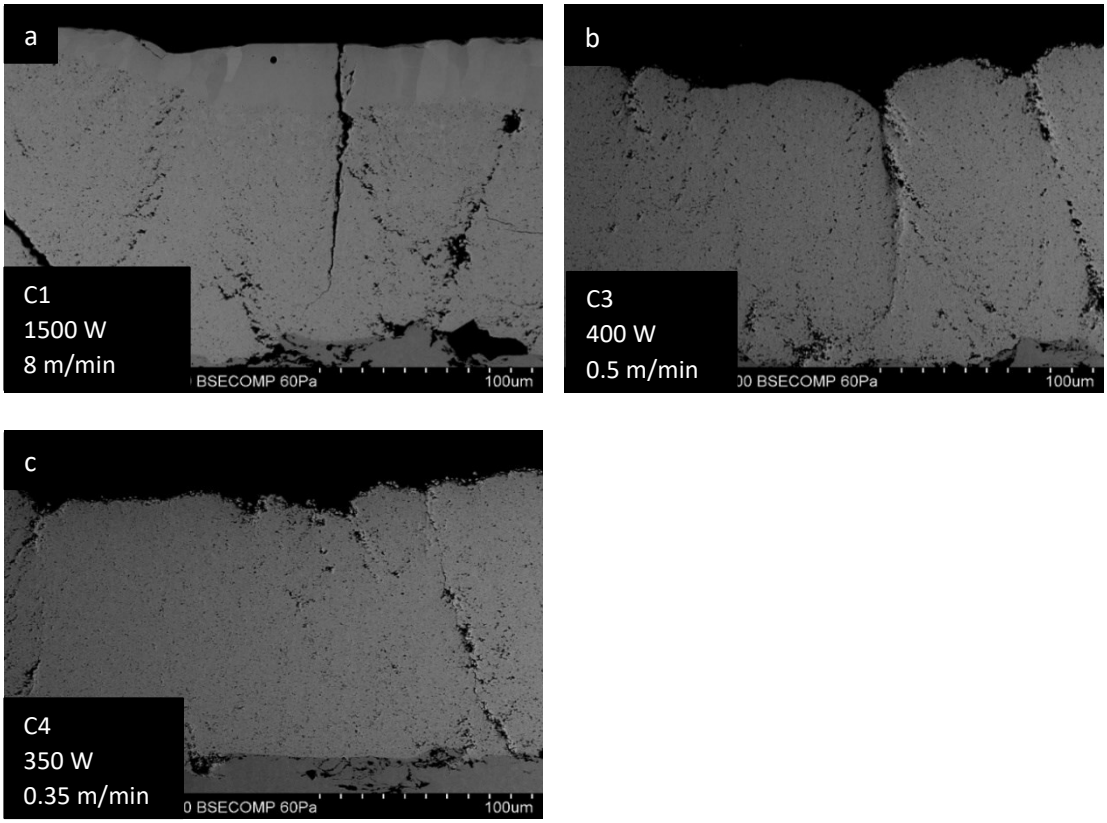

Figure 4-23. SEM image of cross section Test 25, T-L-R- (a) Condition 1 (b) Condition 3 (c) Condition 4

4.2.2 Surface Characterization

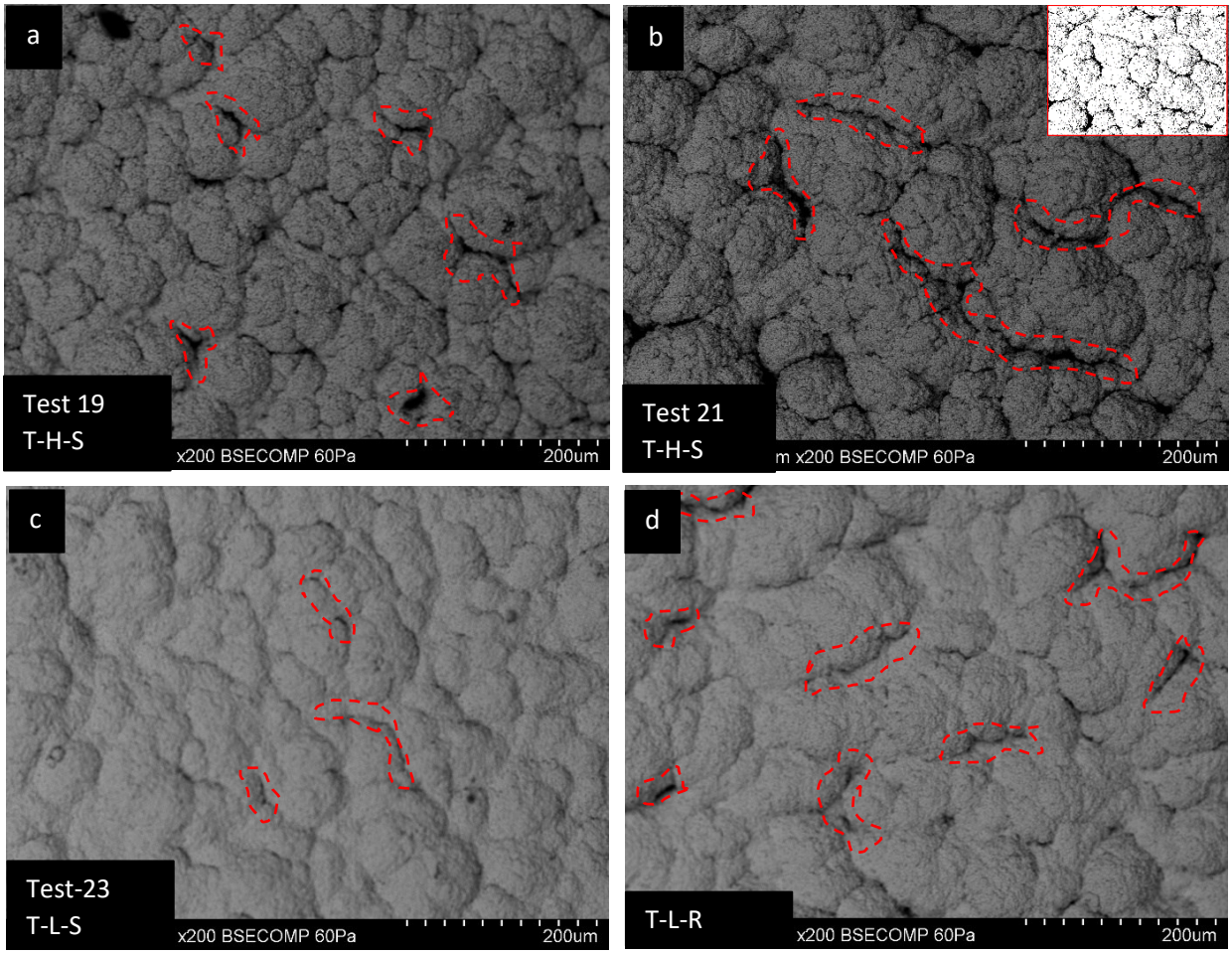

Figure 4-24. SEM image of surface roughness of as-sprayed samples (a) (T-H-S) (b) T-H-R (c) T-L-S (d) T-L-R

One of the laser effects on the surface is related to the surface roughness of the treated zone. As shown in Figure 4-24, all the as-sprayed columnar structures have channels that could allow material from outside penetrate into the coating microstructure. These channels vary depending on each coating (refer to Table 3-4 Columnar structure properties). Based on the analysis done by confocal microscope, as shown in Figure 4-25, the roughness of the surface was reduced from an R_a of 3.4 µm in sample T-H-R in the as-sprayed condition to 0.45 µm after

remelting with 775 W laser power and 1 m/min scanning speed. This condition was selected since it gives a uniform melting all over the substrate.

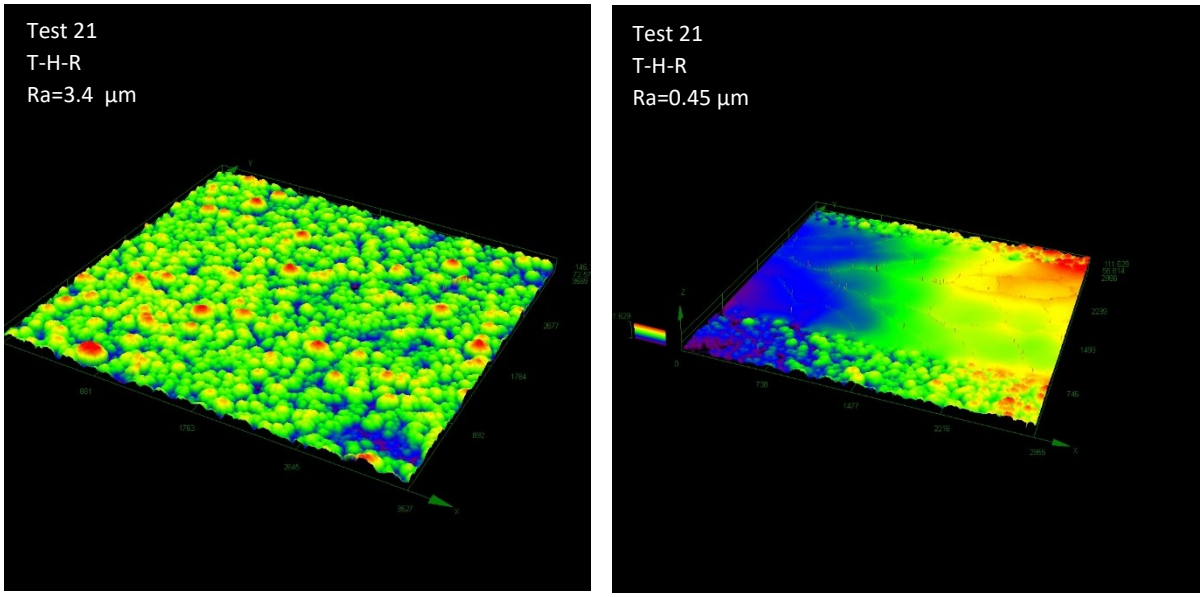

Figure 4-25. Surface roughness obtained by confocal microscope for Test 21 sample T-H-R condition 2- (a) before laser treatment (b) after laser treatment

The cauliflower-like structure with relatively high surface roughness transforms to a flatter surface in terms of surface modification. Melting generates a thin glassy layer on the TBC surface with a crack network across the surface as shown in Figure 4-26. This was the intended objective of this preliminary work into laser remelting of SPS coatings.

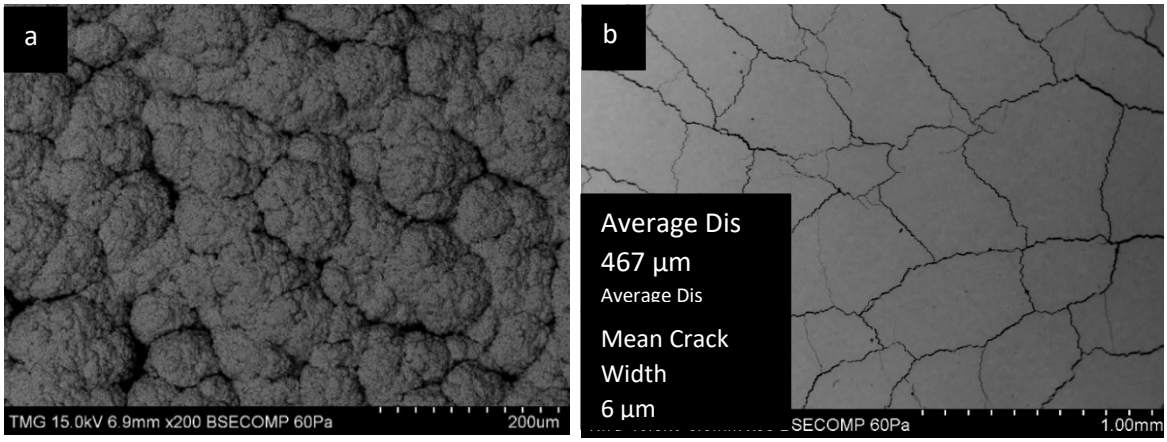

Figure 4-26. Laser remelting on formation of cracks (a) as sprayed Test-21 sample T-H-R (b) Remelted layer under condition 2

4.3 DISCUSSION

This study reveals that laser remelting has the capability of producing a thin remelted layer on top of the porous and columnar structure of the suspension plasma spray coatings; however, consistency of the laser treatment is an issue. The major difficulty is the lack of homogeneity of the remelted areas. Although, reducing scanning speed and considering a specific range of output power may improve the remelted layer quality, it is necessary to consider the spectral properties of YSZ to further improve it.

YSZ has a different absorptivity as a function of wavelength as shown in Figure 4.27[66]. Also figure 4.28 illustrates absorption coefficient plotted as a function of wavelength at four different temperatures for the freestanding plasma-sprayed 8 wt% yttria-stabilized zirconia coatings [67], the wavelength of the 4 kW IPG fiber laser used in this study is 1.07 µm wavelength. At this wavelength, YSZ is highly transparent with a very low absorptivity. In these conditions, we can expect that a large portion of the laser beam is scattered by the pores in the as-sprayed

coatings and only a fraction of the laser power is absorbed by the coating. However, when the YSZ melts, the laser can be efficiently transmitted through the melted YSZ and, then be absorbed by the unmelted coating beneath the YSZ molten pool. As the laser energy is mostly absorbed at the bottom of the molten pool, the melting progresses extremely rapidly and can reach the substrate surface also extremely rapidly making difficult to precisely control the melting process. This is observed in many cases as shown by black zones on many laser-treated coatings.

Using a laser with a longer wavelength around 10 µm, such as a CO_2 laser, may be

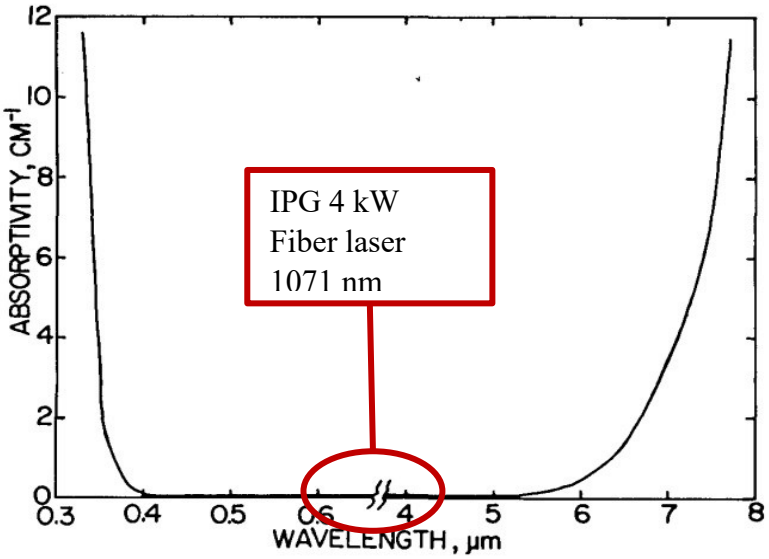

Figure 4-27. Absortivity of cubic zirconia as a function of wavelength

advantageous as, at this wavelength, YSZ has higher absorptivity making the laser energy absorbed at the surface of the coating or the molten pool. In such a case, the propagation of the melting front at the bottom of the molten pool should progress more slowly improving the control of the melted zone during laser treatment.

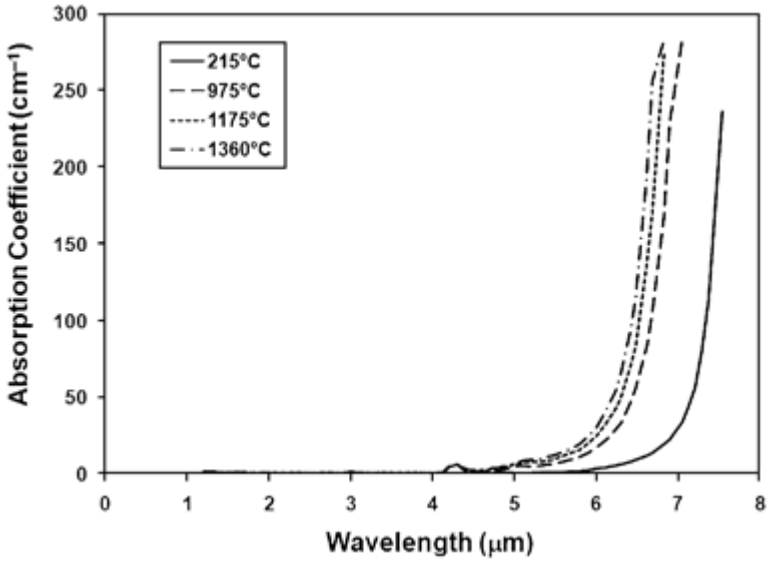

Figure 4-28. Absorption coefficient as a function of wavelength at four different temperatures

Another aspect to discuss is the wetting behaviour of the molten CMAS at the surface of a YSZ coating. The wetting of a liquid on a solid surface is its ability to maintain contact with this solid surface. The wetting behaviour is mostly characterized by the contact angle of the liquid with the solid surface, which relates to the surface energy at the solid-liquid, solid-gas and liquid-gas interfaces.

Normally, the contact angle of liquid CMAS on YSZ single crystal depends the surface Miller index. However, in reality, the surfaces of YSZ TBCs are polycrystalline in nature with many active sites such as interface boundaries, vacancies, and impurities. These surface defects promote the wettability of CMAS on YSZ and affect the contact angle which is not desirable [68], [69]. The surface remelting process and production of a homogeneous melted layer can potentially increase the contact angle and decrease the wettability of the CMAS on YSZ remelted layer limiting the coating degradation.

5 SUMMARY AND CONCLUSIONS

In this study, a suspension plasma spraying process was employed to generate different TBC coating layers under various conditions. Furthermore, laser energy was applied on the coated layer to study the possibility of creating a thin remelted layer on top of a columnar structure. Scanning electron microscopy (SEM) was used to investigate the coated layers and image analysis was used for evaluation.

During the fabrication of columnar microstructures, two suspensions were used: an in-house preparation and a commercial suspension obtained from Treibacher. The structure of the coating prepared with the commercial suspension has considerably higher porosity and a more columnar structure. Substrate roughness had some effect on the formation of the coating microstructure as well, in so much as a substrate with a higher roughness tends to produce more columns from the substrate due to the existence of more asperities on the starting substrate surface than a substrate with lower roughness, which generates a less porous structure and the columns start a distance above the substrate.

The in-house suspension generated a considerable denser structure, with a vertically cracked microstructure. Although increasing surface roughness did increase the porosity somewhat, the columnar structure from the commercial suspension still showed a considerably higher porosity.

The influence of the laser surface treatment on the TBC coating microstructure varied based on the coating structure. This study showed that increasing porosity in the coating structure modifies the laser remelting process.

Laser parameters such as power and scanning speed define the two major parameters that need careful control: power density, and energy density. Power density is independent of scanning speed. Energy density has a direct relation with power and has an inverse relation with scanning speed and as such was shown to have a significant effect on the surface modification

Tests showed that increasing the scanning speed to a range higher than 2 m/min causes local but non-uniform melting of the TBC layer. Even though higher speeds enabled the use of higher laser output power, the coating surface does not have a uniform melting depth. Using a power density of 96 MW/m^2 caused full melting of the TBC and substrate and a power density lower than 43 MW/m^2 did not significantly affect the substrate even at a low range of speeds. Energy densities ranging from 14 J/mm^2 to 19 J/mm^2 have the potential to generate a uniform remelted layer on the TBC surface. A thin remelted layer with narrow cracks was produced as detailed in the scope of this work.

6 FUTURE WORK

This research has contributed to the design and formation of a glassy remelted layer over a columnar structure of YSZ sprayed by the SPS method. In this process, a fiber Nd: YAG laser with a wavelength of λ=1074 nm was used: this wavelength is the near-infrared wavelength and is less absorbed by oxide ceramic powders [6].

Applying this laser on the YSZ material is a relatively new method. Further theoretical and experimental investigations are required to obtain a fully functional and economically optimized method in this regard. Further research in this area can be extended in the following areas:

- The TBC layer used should be increased in thickness to that commonly used in industry: 300 µm to 400 µm. This will mean increasing the number of SPS passes from 20 to 30 or 35 passes. In this case, remelting of 40µm would be a good result.
- As reported in the conclusion section, lowering the scanning speed and increasing the power output, whilst keeping the energy density and power density in a specific range may lead us to obtain optimized results.
- In this research, laser treatment was only applied in one pass. One of the laser parameter's key factors is overlapping; hence this may be studied in future research.
- In this research, the main focus was on obtaining the best condition to obtain the glassy remelted layer. Characterization of such a remelted layer and its effect on the TBC performance would be subsequently needed including mechanical properties of the remelted layer, thermal shock resistance, corrosion, erosion, and hardness behavior.

  • Conducting a detailed life cycle under CMAS exposure.

7 BIBLIOGRAPHY

[1] P. L. Fauchais, J. V. R. Heberlein, and M. I. Boulos, *Thermal Spray Fundamentals*. 2014.

[2] R. Hughes, *Deposition technologies for films and coatings'*, vol. 53, no. 9. 2008.

[3] R. Hughes, *Handbook of thermal spray technology*, vol. 53, no. 9. 2008.

[4] A. Ganvir, *Design of Suspension Plasma Sprayed Thermal Barrier Coatings*, no. 20. 2018.

[5] R. A. Miller, "Thermal barrier coatings for aircraft engines: History and directions," *J. Therm. Spray Technol.*, vol. 6, no. 1, pp. 35–42, 1997, doi: 10.1007/BF02646310.

[6] V. Sankar, "Thermal Barrier Coatings Material Selection , Method of Preparation and Applications - Review," *Int. J. Mech. Eng. Robot. Res.*, vol. 3, no. 2, pp. 510–517, 2014.

[7] A. Ganvir, R. F. Calinas, N. Markocsan, N. Curry, and S. Joshi, "Experimental visualization of microstructure evolution during suspension plasma spraying of thermal barrier coatings," *J. Eur. Ceram. Soc.*, vol. 39, no. 2–3, pp. 470–481, 2019, doi: 10.1016/j.jeurceramsoc.2018.09.023.

[8] R. Vaßen, M. O. Jarligo, T. Steinke, D. E. Mack, and D. Stöver, "Overview on advanced thermal barrier coatings," *Surf. Coatings Technol.*, vol. 205, no. 4, pp. 938–942, 2010, doi: 10.1016/j.surfcoat.2010.08.151.

[9] R. Ahmadi-Pidani, R. Shoja-Razavi, R. Mozafarinia, and H. Jamali, "Laser surface modification of plasma sprayed CYSZ thermal barrier coatings," *Ceram. Int.*, vol. 39, no. 3, pp. 2473–2480, 2013, doi: 10.1016/j.ceramint.2012.09.005.

[10] R. Vassen, X. Cao, F. Tietz, D. Basu, and D. Stöver, "Zirconates as new materials for thermal barrier coatings," *J. Am. Ceram. Soc.*, vol. 83, no. 8, pp. 2023–2028, 2000, doi: 10.1111/j.1151-2916.2000.tb01506.x.

[11] D. Zhou, *Columnar Structured Thermal Barrier Coatings Deposited by Axial Suspension*

Plasma Spraying, vol. 456. 2019.

[12] R. F. Bunshah, *HANDBOOK OF DEPOSITION TECHNOLOGIES and Applications Edited by*. .

[13] J. Singh and D. E. Wolfe, "Nano and macro-structured component fabrication by electron beam-physical vapor deposition (EB-PVD)," *J. Mater. Sci.*, vol. 40, no. 1, pp. 1–26, 2005, doi: 10.1007/s10853-005-5682-5.

[14] R. B. Heimann, *Plasma- Spray Coating*. .

[15] A. A. Kulkarni *et al.*, "Advanced microstructural characterization of plasma-sprayed zirconia coatings over extended length scales," *J. Therm. Spray Technol.*, vol. 14, no. 2, pp. 239–250, 2005, doi: 10.1361/10599630523818.

[16] "ASM HANDBOOK Volume 5 Surface Engineering."

[17] B. Bernard *et al.*, "Thermal insulation properties of YSZ coatings: Suspension Plasma Spraying (SPS) versus Electron Beam Physical Vapor Deposition (EB-PVD) and Atmospheric Plasma Spraying (APS)," *Surf. Coatings Technol.*, vol. 318, pp. 122–128, 2017, doi: 10.1016/j.surfcoat.2016.06.010.

[18] A. Ganvir, N. Curry, S. Björklund, N. Markocsan, and P. Nylén, "Characterization of Microstructure and Thermal Properties of YSZ Coatings Obtained by Axial Suspension Plasma Spraying (ASPS)," *J. Therm. Spray Technol.*, vol. 24, no. 7, pp. 1195–1204, 2015, doi: 10.1007/s11666-015-0263-x.

[19] J. Knuuttila, P. Sorsa, and T. Mäntylä, "Sealing of thermal spray coatings by impregnation," *J. Therm. Spray Technol.*, vol. 8, no. 2, pp. 249–257, 1999, doi: 10.1007/s11666-999-0002-2.

[20] I. Berezin and T. Troczynski, "Surface modification of zirconia thermal barrier coatings," *J. Mater. Sci. Lett.*, vol. 15, no. 3, pp. 214–218, 1996, doi: 10.1007/BF00274454.

[21] K. A. Khor and Y. W. Gu, "Hot isostatic pressing of plasma sprayed yttria-stabilized zirconia," *Mater. Lett.*, vol. 34, no. 3–6, pp. 263–268, 1998, doi: 10.1016/S0167-577X(97)00184-5.

[22] P. Vuoristo and P. Kettunen, “437 c h e m i c a l vapour d e p o s i t i o n d e n s i f i c a t i o n o f plasma- sprayed oxide c o a t i n g s *,” vol. 118, pp. 437–444, 1984.

[23] R. Rajendran, V. S. Raja, R. Sivakumar, and R. S. Srinivasa, “Reduction of interconnected porosity in zirconia-based thermal barrier coating,” *Surf. Coatings Technol.*, vol. 73, no. 3, pp. 198–200, 1995, doi: 10.1016/0257-8972(94)02368-9.

[24] A. Y. C. Nee, *Handbook of manufacturing engineering and technology*. 2015.

[25] A. H. Rawicz, “Theodore Harold Maiman and the invention of laser,” *Photonics, Devices, Syst. IV*, vol. 7138, p. 713802, 2008, doi: 10.1117/12.817966.

[26] A. H. Ion, “Introduction,” *War Dipl. Across Pacific, 1919-1952*, pp. 1–20, 2006, doi: 10.1016/b978-075066079-2/50004-0.

[27] C. Batista, A. Portinha, R. M. Ribeiro, V. Teixeira, M. F. Costa, and C. R. Oliveira, “Surface laser-glazing of plasma-sprayed thermal barrier coatings,” *Appl. Surf. Sci.*, vol. 247, no. 1–4, pp. 313–319, 2005, doi: 10.1016/j.apsusc.2005.01.047.

[28] A. Killinger, R. Gadow, G. Mauer, A. Guignard, R. Vaen, and D. Stöver, “Review of new developments in suspension and solution precursor thermal spray processes,” *J. Therm. Spray Technol.*, vol. 20, no. 4, pp. 677–695, 2011, doi: 10.1007/s11666-011-9639-8.

[29] L. Pawlowski, “Suspension and solution thermal spray coatings,” *Surf. Coatings Technol.*, vol. 203, no. 19, pp. 2807–2829, 2009, doi: 10.1016/j.surfcoat.2009.03.005.

[30] A. Bacciochini, G. Montavon, J. Ilavsky, A. Denoirjean, and P. Fauchais, “Porous architecture of SPS thick YSZ coatings structured at the nanometer scale (∼50 nm),” *J. Therm. Spray Technol.*, vol. 19, no. 1–2, pp. 198–206, 2010, doi: 10.1007/s11666-009-9429-8.

[31] K. Vanevery *et al.*, “Column formation in suspension plasma-sprayed coatings and resultant thermal properties,” *J. Therm. Spray Technol.*, vol. 20, no. 4, pp. 817–828, 2011, doi: 10.1007/s11666-011-9632-2.

[32] F. Caio and C. Moreau, “Influence of substrate shape and roughness on coating microstructure in Suspension Plasma Spray,” *Coatings*, vol. 9, no. 11, 2019, doi:

10.3390/coatings9110746.

[33] R. Kromer, P. Sokołowski, R. T. Candidato, S. Costil, and L. Pawłowski, “SPS coating microstructure controlled by the surface topography using laser texturing,” *Proc. Int. Therm. Spray Conf.*, vol. 1, no. June, pp. 158–172, 2017.

[34] A. Ganvir *et al.*, “Influence of Microstructure on Thermal Properties of Axial Suspension Plasma-Sprayed YSZ Thermal Barrier Coatings,” *J. Therm. Spray Technol.*, vol. 25, no. 1–2, pp. 202–212, 2016, doi: 10.1007/s11666-015-0355-7.

[35] R. Chidambaram Seshadri, G. Dwivedi, V. Viswanathan, and S. Sampath, “Characterizing Suspension Plasma Spray Coating Formation Dynamics through Curvature Measurements,” *J. Therm. Spray Technol.*, vol. 25, no. 8, pp. 1666–1683, 2016, doi: 10.1007/s11666-016-0460-2.

[36] A. Ganvir, S. Joshi, N. Markocsan, and R. Vassen, “Tailoring columnar microstructure of axial suspension plasma sprayed TBCs for superior thermal shock performance,” *Mater. Des.*, vol. 144, pp. 192–208, 2018, doi: 10.1016/j.matdes.2018.02.011.

[37] A. Ganvir, N. Markocsan, and S. Joshi, “Influence of isothermal heat treatment on porosity and crystallite size in axial suspension plasma sprayed thermal barrier coatings for gas turbine applications,” *Coatings*, vol. 7, no. 1, 2017, doi: 10.3390/coatings7010004.

[38] D. Zhou, O. Guillon, and R. Vaßen, “Development of YSZ thermal barrier coatings using axial suspension plasma spraying,” *Coatings*, vol. 7, no. 8, 2017, doi: 10.3390/coatings7080120.

[39] Z. Tang, H. Kim, I. Yaroslavski, G. Masindo, Z. Celler, and D. Ellsworth, “Novel Thermal Barrier Coatings Produced by Axial Suspension Plasma Spray (b) (c) (a),” *Proc. Int. Therm. Spray Conf. Expo.*, pp. 1–5, 2011.

[40] V. Akdoğan, M. M. Dokur, G. Göller, and Ö. Keles, “Surface modification of thermal barrier coatings by single-shot defocused laser treatments,” *J. Mater. Eng. Perform.*, vol. 22, no. 9, pp. 2500–2509, 2013, doi: 10.1007/s11665-013-0548-5.

[41] W. M. Steen and J. Powell, “Laser surface treatment,” *Mater. Des.*, vol. 2, no. 3, pp. 157–162, 1981, doi: 10.1016/0261-3069(81)90056-X.

[42] H. L. Tsai and P. C. Tsai, “Laser Glazing of Plasma-Sprayed Zirconia Coatings,” *J. Mater. Eng. Perform.*, vol. 7, no. 2, pp. 258–264, 1998, doi: 10.1361/105994998770347990.

[43] C. Batista, A. Portinha, R. M. Ribeiro, V. Teixeira, M. F. Costa, and C. R. Oliveira, “Morphological and microstructural characterization of laser-glazed plasma-sprayed thermal barrier coatings,” *Surf. Coatings Technol.*, vol. 200, no. 9, pp. 2929–2937, 2006, doi: 10.1016/j.surfcoat.2004.10.134.

[44] P. C. Tsai and C. S. Hsu, “High temperature corrosion resistance and microstructural evaluation of laser-glazed plasma-sprayed zirconia/MCrAlY thermal barrier coatings,” *Surf. Coatings Technol.*, vol. 183, no. 1, pp. 29–34, 2004, doi: 10.1016/j.surfcoat.2003.08.090.

[45] R. Ahmadi-Pidani, R. Shoja-Razavi, R. Mozafarinia, and H. Jamali, “Improving the thermal shock resistance of plasma sprayed CYSZ thermal barrier coatings by laser surface modification,” *Opt. Lasers Eng.*, vol. 50, no. 5, pp. 780–786, 2012, doi: 10.1016/j.optlaseng.2011.12.007.

[46] M. G. Gok and G. Goller, “Microstructural evaluation of laser remelted gadolinium zirconate thermal barrier coatings,” *Surf. Coatings Technol.*, vol. 276, pp. 202–209, 2015, doi: 10.1016/j.surfcoat.2015.06.074.

[47] M. F. Morks, C. C. Berndt, Y. Durandet, M. Brandt, and J. Wang, “Microscopic observation of laser glazed yttria-stabilized zirconia coatings,” *Appl. Surf. Sci.*, vol. 256, no. 21, pp. 6213–6218, 2010, doi: 10.1016/j.apsusc.2010.03.143.

[48] Z. Fan *et al.*, “Influence of columnar grain microstructure on thermal shock resistance of laser re-melted ZrO2-7wt.% Y2O3 coatings and their failure mechanism,” *Surf. Coatings Technol.*, vol. 277, no. July, pp. 188–196, 2015, doi: 10.1016/j.surfcoat.2015.07.036.

[49] Y. Feng *et al.*, “The roles of stress in the thermal shock failure of YSZ TBCs before and after laser remelting,” *J. Alloys Compd.*, vol. 828, 2020, doi: 10.1016/j.jallcom.2020.154417.

[50] H. Chen, Y. Hao, H. Wang, and W. Tang, “Analysis of the microstructure and thermal

shock resistance of laser glazed nanostructured zirconia TBCs," *J. Therm. Spray Technol.*, vol. 19, no. 3, pp. 558–565, 2010, doi: 10.1007/s11666-009-9463-6.

[51] P. Yi *et al.*, "Effects of laser surface remelting on the molten salt corrosion resistance of yttria-stabilized zirconia coatings," *Ceram. Int.*, vol. 44, no. 18, pp. 22645–22655, 2018, doi: 10.1016/j.ceramint.2018.09.041.

[52] R. Ghasemi, R. Shoja-Razavi, R. Mozafarinia, H. Jamali, M. Hajizadeh-Oghaz, and R. Ahmadi-Pidani, "The influence of laser treatment on hot corrosion behavior of plasma-sprayed nanostructured yttria stabilized zirconia thermal barrier coatings," *J. Eur. Ceram. Soc.*, vol. 34, no. 8, pp. 2013–2021, 2014, doi: 10.1016/j.jeurceramsoc.2014.01.031.

[53] Z. Yan, L. Guo, Z. Li, Y. Yu, and Q. He, "Effects of laser glazing on CMAS corrosion behavior of Y2O3 stabilized ZrO2 thermal barrier coatings," *Corros. Sci.*, vol. 157, no. May, pp. 450–461, 2019, doi: 10.1016/j.corsci.2019.06.025.

[54] K. Poorna Chander, M. Vashista, K. Sabiruddin, S. Paul, and P. P. Bandyopadhyay, "Effects of grit blasting on surface properties of steel substrates," *Mater. Des.*, vol. 30, no. 8, pp. 2895–2902, 2009, doi: 10.1016/j.matdes.2009.01.014.

[55] R. Rampon, O. Marchand, C. Filiatre, and G. Bertrand, "Influence of suspension characteristics on coatings microstructure obtained by suspension plasma spraying," *Surf. Coatings Technol.*, vol. 202, no. 18, pp. 4337–4342, 2008, doi: 10.1016/j.surfcoat.2008.04.006.

[56] N. Curry, K. VanEvery, T. Snyder, J. Susnjar, and S. Bjorklund, "Performance testing of suspension plasma sprayed thermal barrier coatings produced with varied suspension parameters," *Coatings*, vol. 5, no. 3, pp. 338–356, 2015, doi: 10.3390/coatings5030338.

[57] J. Fazilleau, C. Delbos, V. Rat, J. F. Coudert, P. Fauchais, and B. Pateyron, "Phenomena involved in suspension plasma apraying part 1: Suspension injection and behavior," *Plasma Chem. Plasma Process.*, vol. 26, no. 4, pp. 371–391, 2006, doi: 10.1007/s11090-006-9019-1.

[58] Y. S. Zirconia, "AuerCoat ® YSZ Suspension AuerCoat ® YSZ Suspension Yttria Stabilized Zirconia , suspension in ethanol."

[59] A. C. Solutions, “Axial III ^{TM} Spray System - Advanced Coating Solutions,” *Time*.

[60] “Mettech 350 feeder.” https://www.mettech.com/assets/pdf/brochure_nanofeed.pdf.

[61] IPG Photonics Corporation, “ipgphotonics.” https://www.ipgphotonics.com/en/products/lasers/high-power-cw-fiber-lasers.

[62] IPG Photonics Corporation, “High Power Fiber Laser User Guide,” 2014.

[63] E. Bakan and R. Vaßen, “Ceramic Top Coats of Plasma-Sprayed Thermal Barrier Coatings: Materials, Processes, and Properties,” *J. Therm. Spray Technol.*, vol. 26, no. 6, pp. 992–1010, 2017, doi: 10.1007/s11666-017-0597-7.

[64] S. Morelli *et al.*, “CMAS corrosion of YSZ thermal barrier coatings obtained by different thermal spray processes,” *J. Eur. Ceram. Soc.*, vol. 40, no. 12, pp. 4084–4100, 2020, doi: 10.1016/j.jeurceramsoc.2020.04.058.

[65] N. Curry, K. VanEvery, T. Snyder, and N. Markocsan, “Thermal conductivity analysis and lifetime testing of suspension plasma-sprayed thermal barrier coatings,” *Coatings*, vol. 4, no. 3, pp. 630–650, 2014, doi: 10.3390/coatings4030630.

[66] D. L. Wood and K. Nassau, “Refractive index of cubic zirconia stabilized with yttria,” *Appl. Opt.*, vol. 21, no. 16, p. 2978, 1982, doi: 10.1364/ao.21.002978.

[67] J. I. Eldridge, C. M. Spuckler, and J. R. Markham, “Determination of scattering and absorption coefficients for plasma-sprayed yttria-stabilized zirconia thermal barrier coatings at elevated temperatures,” *J. Am. Ceram. Soc.*, vol. 92, no. 10, pp. 2276–2285, 2009, doi: 10.1111/j.1551-2916.2009.03217.x.

[68] W. Song, Y. Lavallée, F. B. Wadsworth, K. U. Hess, and D. B. Dingwell, “Wetting and Spreading of Molten Volcanic Ash in Jet Engines,” *J. Phys. Chem. Lett.*, vol. 8, no. 8, pp. 1878–1884, 2017, doi: 10.1021/acs.jpclett.7b00417.

[69] B. Li, Z. Chen, H. Zheng, G. Li, H. Li, and P. Peng, “Wetting mechanism of CMAS melt on YSZ surface at high temperature: First-principles calculation,” *Appl. Surf. Sci.*, vol. 483, no. March, pp. 811–818, 2019, doi: 10.1016/j.apsusc.2019.04.009.

[70] B. Bernard *et al.*, “Thermal insulation properties of YSZ coatings: Suspension Plasma

Spraying (SPS) versus Electron Beam Physical Vapor Deposition (EB-PVD) and Atmospheric Plasma Spraying (APS),” *Surf. Coatings Technol.*, vol. 318, pp. 122–128, 2017, doi: 10.1016/j.surfcoat.2016.06.010.